Jerald M. Vogel

M. Gawad Nagati

WING/BODY INTERFERENCE FLOW INVESTIGATION

Final Technical Report

NASA Contract NCC 2-19

ERI Project 1432

engineering research institute

iowa state university

Vortex sheet modeling with

higher order curved panels

by

M. Gawad Nagati

A Dissertation Submitted to the

Graduate Faculty in Partial Fulfillment of the

Requirements for the Degree of

DOCTOR OF PHILOSOPHY

Major: Aerospace Engineering

Approved:

Members of the Committee

_____
In Charge of Major Work

_____
For the Major Department

_____
For the Graduate College

Iowa State University
Ames, Iowa

TABLE OF CONTENTS

LIST OF SYMBOLS

a	coefficients of patch polynomials
b	wing span
c	local wing chord
C_ℓ	local section lift coefficient
C	curve
$\mathcal{D}$	domain of irrotational flow
i,j	node or patch indices
k,ℓ	powers of u,v in polynomials
m,n	rectangular patch network size
M	Mach number
$\hat{n}$	unit normal vector
P	field point
Q	singularity point or coefficient matrix
$\vec{r}$	relative position vector
s	arc length of a curve
t	time lapsed
$\vec{t}$	unit tangent vector
u,v	parameters used in interpolants
$\vec{V}$	induced velocity vector at a point - Components of $\vec{V}$ are: V_x, V_y, V_z.
V_∞	free stream velocity
X	matrix of patch node positions and tangent vectors
$\vec{x}$	position vector of point Q, with coordinates x,y,z

α angle of attack

β sideslip angle

γ vorticity strength

Γ circulation $= \int \gamma dS$

δ, Δ increment

θ angle

ϕ potential function

∇^2 Laplacian operator

$\vec{\xi}$ position vector of point P, with components ξ, η, ζ

σ source strength

μ doublet strength

ρ magnitude of relative position vector

$\iint\limits_S$ surface integral over area S

Subscripts

u,v   partial differentiation

CHAPTER 1: INTRODUCTION

Scope

Potential flow methods have been used successfully for the last two decades in the preliminary design of partial or complete aircraft configurations. Predictions by numerical schemes based on potential flow analyses include such aerodynamic characteristics as wing load distributions, surface pressure distributions, engine duct flows, and some stability derivatives, among others.

Results of such computations concerning surfaces affected by trailing vortex sheets of lifting surfaces are correct only for simple configurations where the effects of the location and shape of the vortex sheet are secondary. The shape of the vortex sheet is usually assumed to be flat. Realistically, however, its configuration changes continuously in the downstream direction at least until roll-up of the sheet into concentrated vortex cores is complete. The process of roll-up is rather complex. Mutual interaction among the elements of the sheet depends on their relative positions, however, the configuration of the sheet is unknown prior to the complete solution including its effect.

Much of the change in the sheet shape occurs within a downstream distance from the generating wing equal to half the wingspan. The purpose of this study is to develop a

numerical technique of modeling the vortex sheet with a deformable surface definition, along which a continuous vortex strength distribution in the spanwise direction is applied, so that by repeatedly modifying its shape, its true configuration is approached, in the proximity of its generating wing.

Design problems requiring the inclusion of a realistic configuration of the vortex sheet are numerous. Some examples are discussed in the following.

Control effectiveness and stability derivatives

In the early stages of aircraft design, horizontal and vertical stabilizers must be sized fairly accurately to ensure aircraft controllability within the flight envelope. Downwash and sidewash angles at zero angles of attack and sideslip and their rates of change with these angles are predicted in practice using empirical relations (reference 11 and 31, for example) which are not based on general aircraft configurations, but rather on crude parameters such as wing sweep and dihedral angles, aspect ratio, etc. The real governing factor is the wing loading distribution and changes in it with Mach Number and attitude with respect to free stream direction. This distribution results in a free vortex sheet extending in theory from the trailing edge of the generating wing to an infinite distance downstream of the wing. The vorticity is constant streamwise, and varies with

chordwise distance. Roll-up of the sheet occurs about areas of concentrated vorticity called the vortex cores (4, 23) and if in the vicinity of the empennage, such cores will affect surface pressure distributions. Two cases are represented.

Longitudinal stability   As illustrated in Figure 1, the deflected flaps of the aircraft result in a redistribution of lift on the wing, and thus a concentrated vortex core pair emanates at the outboard edge of the flaps that drastically changes the downwash at the horizontal stabilizer. Shock induced separation of the outer wing panel in transonic aircraft causes a similar effect, which aggravates the instability due to the forward displacement of the center of lift of a sweptback wing.

Lateral stability   Figure 2 depicts a yawed twin-engine aircraft. The dip in the wing lift distribution due to the nacelles, caused by inviscid as well as viscous effects, leads to a pair of concentrated vortex cores which are not symmetric due to yaw. The sidewash angle distribution along the stabilizer is altered. In addition, the left side of the rear fuselage is closer to center of the inboard left vortex than the right side is to the center of the inboard right vortex. A pressure differential and thus a destabilizing yawing moment result.

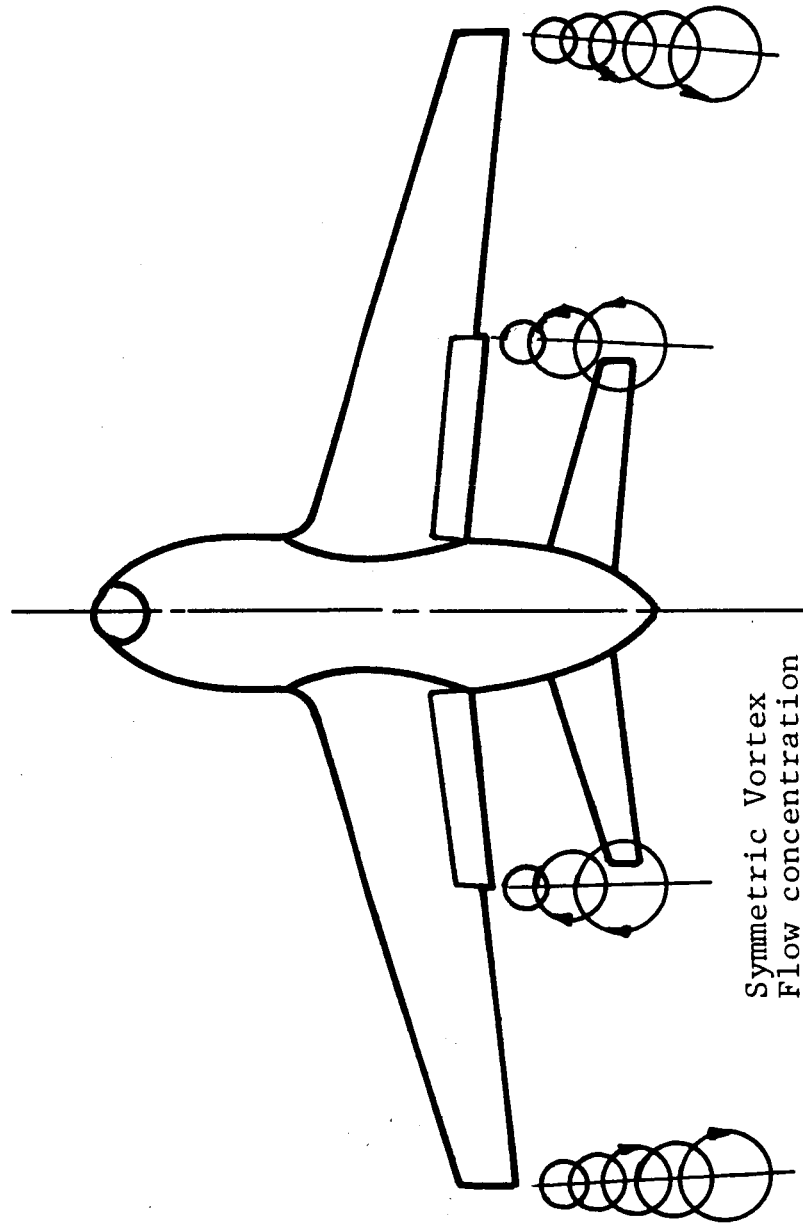Symmetric Vortex
Flow concentration

Figure 1. Longitudinal destabilization due to complex
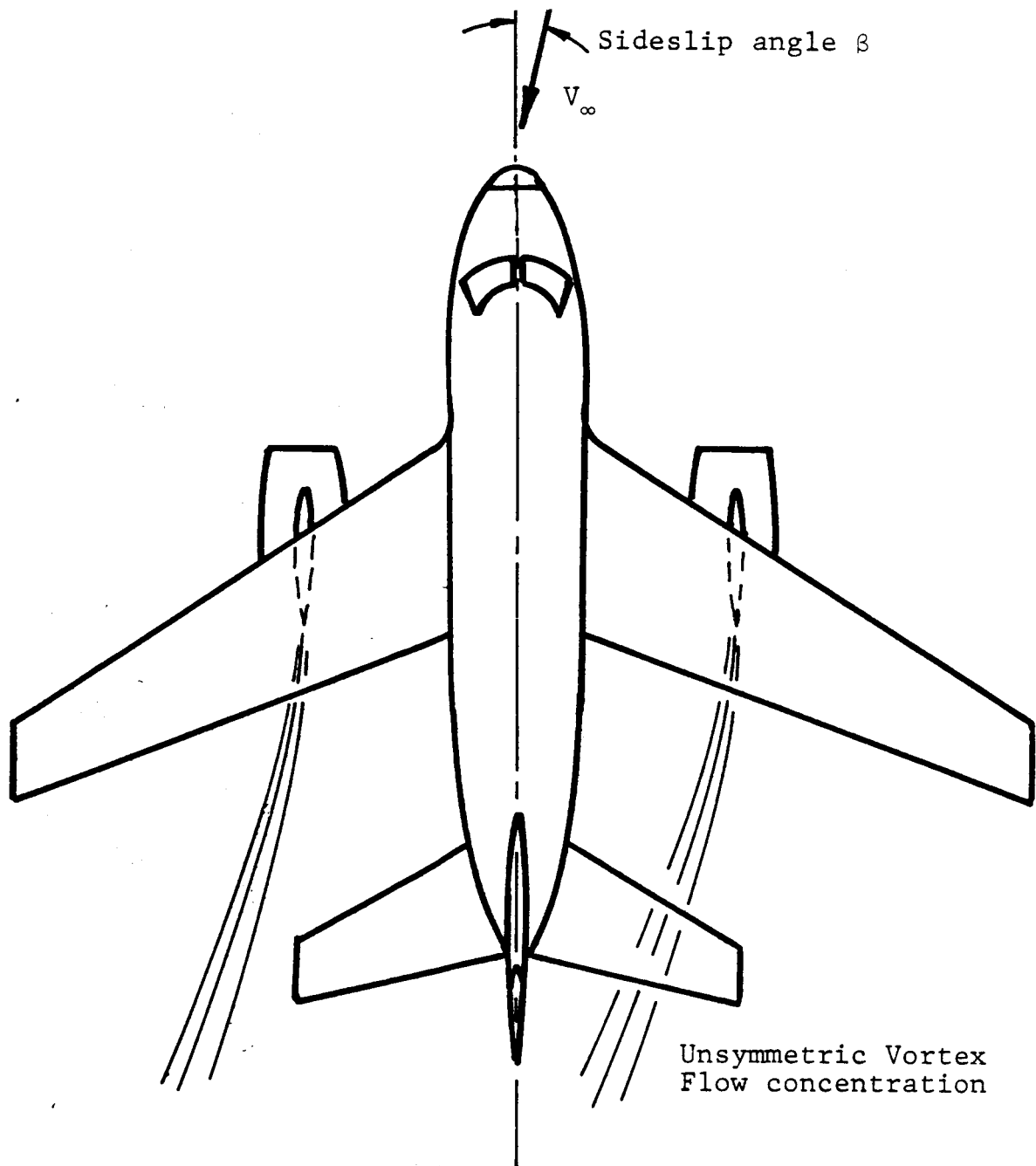wing loading resulting from flap deployment.

Figure 2. Lateral destabilization due to nacelle side forces and complex wing loading

Canards

An effect similar to the above should be investigated for canard-configured aircraft. The vorticity from the canard could affect the lift distribution of the main lifting wing, and subsequently alter the aerodynamic performance of the wing under certain conditions.

Propellers and helicopters rotors

Good aerodynamic design for propeller or rotor afterbodies (nacelles and other solid boundary surfaces) requires simultaneous consideration of all components. The effect of these lifting surfaces is felt on other solid boundaries through the vortex sheets they shed. Therefore, a more detailed knowledge of the shape of the vortex sheet and hence the induced flow field is necessary. For these cases, a quasi-static analysis is required. Such studies are also necessary for designs which must result in low aerodynamic noise.

Trailing vortex hazard

Although this area has been studied extensively recently (7, 9, 23), the present method could be extended to its treatment, insofar as determining the locations and intensities of each of the trailing vortex cores. The interest in this case is primarily in the far downstream region and to promote early dissipation of vortex energy. Farther downstream,

viscous effects become more pronounced, and since the
current method is inviscid, vortex merging and dissipation
must be treated by some other means. Nevertheless, it is
necessary to establish the initial roll-up which is essen-
tially inviscid, to enable the treatment of merging and
dissipation.

Background

The present method is based upon earlier work in three
major areas of computational methods, all of which have
undergone considerable development in the last two decades.
A brief historical review is presented in this section.

Panel methods

In the early sixties, a computational method was devel-
oped to predict nonlifting potential flow about arbitrary
three-dimensional bodies by placing a source distribution on
the outer surface of the body. The source strength is approx-
imated by piecewise constant strength over flat "panels"
which approximate the body surface (15). At about the same
time, vortex lattice methods were being developed (26) for
very thin lifting surfaces. The approach is similar except
that the camber surface of a lifting wing is represented and
a discrete horseshoe vortex lattice is used. Later, the two
techniques were combined to solve arbitrary three-dimensional
lifting potential flow configuration problems. Examples of

work published in this area include those of Rubbert and
Saaris (28). The solution of the flow is obtained by solv-
ing for the singularity (source and doublet) strength dis-
tributions on the entire surface. The problem is reduced
to a set of simultaneous linear equations which can be solved
non-trivially by imposing Neumann boundary conditions at the
solid boundaries and the Kutta condition at the lifting sur-
face trailing edges. The induced effects on the surface or
elsewhere can then be calculated. More recent developments
were directed to higher order singularity (source and doublet)
distributions, in order to improve the predictions and also to
facilitate surface paneling (20). Excessive care for the
panel arrangement is thus no longer required.

In the present study, the doublet (or vortex) strength
distributions are known (obtained by some panel technique)
for the test wing. The spanwise distribution remains the
same along the sheet at any streamwise station, downstream
of the trailing edge. The same type of doublet distribution
panels are used to determine induced effects to obtain the
rolled-up shape, except that these panels are constantly
reshaped and refitted.

Vortex sheet roll-up

A comprehensive survey of computational methods for
lift-generated wakes is given by Rossow (23). The vortex
sheet (or wake) trailing behind the generating wing is divid-

ed in three regions: roll-up, plateau, and decay. In this study, the roll-up region is the one of interest. The problem of roll-up was addressed by Betz (4), then by Westwater (32), where approximations were introduced to eliminate the unnecessary complications of viscous effects. Many techniques have been developed since to overcome the shortcomings using artificial means. The major problem was the use of discrete vortices to approximate the vortex sheet, rather than a continuous distribution as the present method proposes.

The interest in obtaining the rolled-up shape of the wake was motivated by the advent of large aircraft. The wake left by a Boeing 747 for example, during climb or descent is extremely hazardous for following aircraft and extends for several kilometers. Many of the methods developed have been intended for finding means of alleviating that hazard, such as by modifying the wing loading of the generating aircraft to prevent or reduce vortex merging (part of the roll-up mechanism for complex wing loading) and thus speed up the decay process.

Parametric bicubic surface representation

Representation of general curved surfaces was developed for computer aided design of aircraft (13) and automobiles (5). It is necessary in this study to use curved panels, and it was found that the Ferguson patches are best suited for modeling the vortex sheet surface.

General Description of the Proposed Technique

Since the purpose of this method is to establish the shape of the trailing vortex sheet in the vicinity of the wing, it is assumed that the strength of the vortex sheet is known. Curved and deformable panels of known piecewise linear vorticity strength distribution (equivalent to quadratic doublet distribution) are patched together to simulate the vortex sheet, (Figure 3). The geometry of these panels is modeled by using parametric bicubic patches with second derivative continuity (C^2) across their boundaries.

Initially, the surface is flat. The induced velocity at each node in the network is calculated, and some nodes can be displaced accordingly, resulting in a new shape, with the remaining nodes following. The procedure is repeated with the new shape until the entire surface has been relaxed to the final shape. (A complete description is in Chapter 4.)

These induced velocities can include the effects of the bound and free doublet panels as well as any solid boundary whose consideration is desirable, such as a fuselage, trailing lifting surface, nacelle, etc. However, the solution for the entire flow must be re-computed at each relaxation step. In this study, only the doublet panels of the trailing and bound vorticity are considered, since the inclusion of other bodies is merely a programming and computing effort. In

Generating wing
bound vortex panels
(Roman numerals)

Wake or free
vortex sheet panels
(Arabic numerals)

Aircraft
plane of
symmetry

I,I

II,I

I,II

1,1

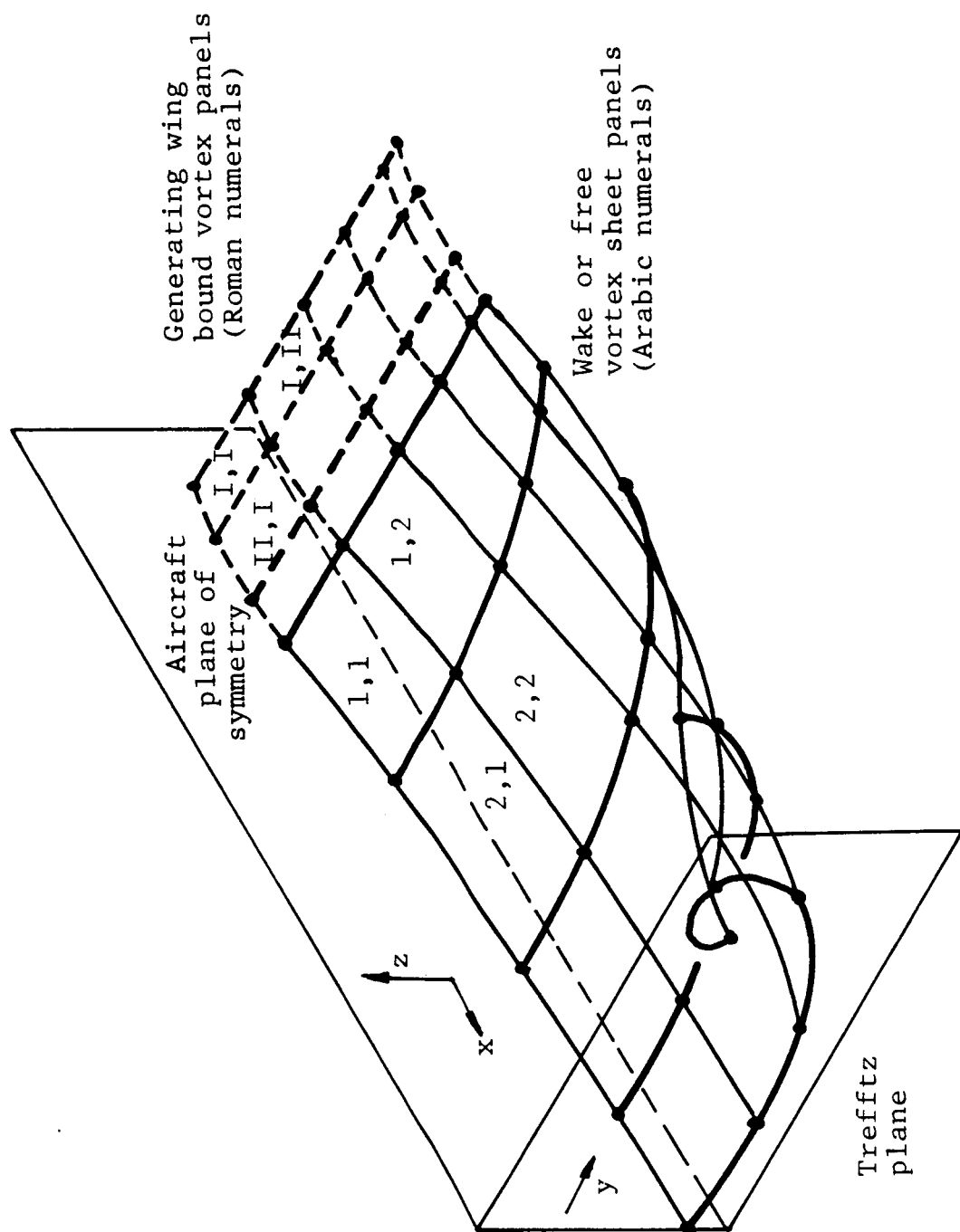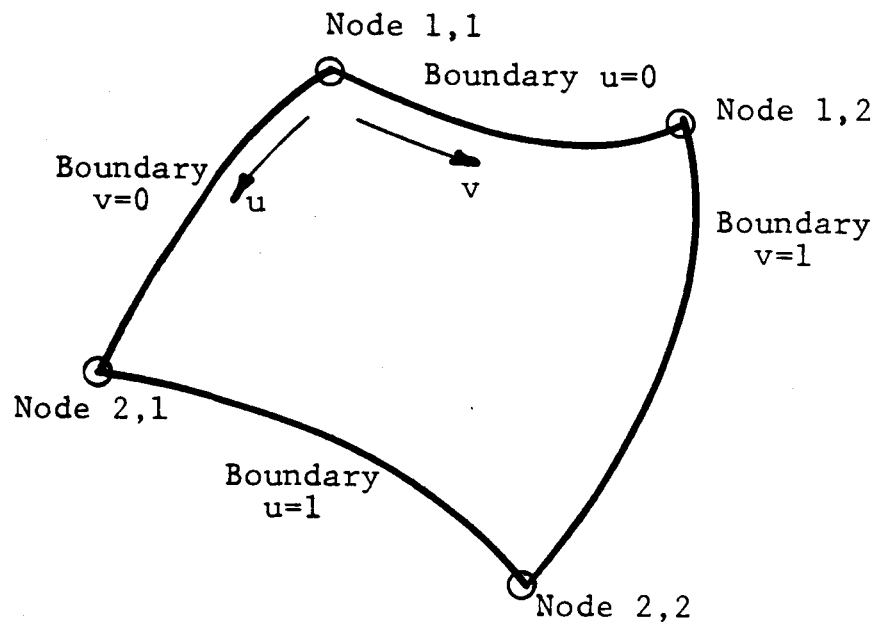1,2

2,1

2,2

z

x

y

Trefftz
plane

Figure 3. Panel network to simulate vortex sheet and
coordinate system

u and v are the parameters
in the bicubic expression
for physical coordinates.

Figure 4.   Panel nomenclature

addition, the roll-up effect on the lift distribution on the generating wing itself is assumed to be negligible (30).

Flow Idealizations Summary

The following assumptions are made in this study:

Potential flow   The flow is everywhere irrotational and incompressible except at the boundary surfaces (specifically the vortex sheet).

Symmetry of the generating wing and vortex sheet Sideslip could easily be included for yawed configurations.

Inviscid flow   The viscous effects become pronounced downstream of the area of concern.

Tip flow   No tip flow for the wing is considered, since the wing character itself is not of primary concern, although its loading near the tip will be somewhat affected.

Steady state   Oscillatory and other time-dependent flows must be treated quasi-statically if this technique is to be used.

Wing lift distribution   The wing lift distribution is based on the assumption of a flat trailing vortex sheet. As indicated above, the roll-up effect is negligible at least for the purpose of this study. In Rossow (23), noticeable effects are shown which could be included with considerably more computational effort.

CHAPTER II: VORTEX SHEET GEOMETRY

The vortex sheet is mathematically considered to be a surface of finite width extending from the lifting surface to infinity, across which there is a jump in the potential function ϕ. This jump in ϕ is equal to the doublet strength. The surface must be represented by a mathematical model which provides for at least slope continuity and allows for the curled or spiral shape of the rolled-up sheet including infinite slope tangents, as well as slope constraints at the edges of the sheet.

Parametric Bicubic Representation

The position vector $\vec{x} \equiv (x,y,z)$ of a point P on the surface within one patch is given by the interpolant

$$\vec{x} = \sum_{k=0}^{3} \sum_{\ell=0}^{3} \vec{a}_{k\ell} u^k v^\ell \tag{1}$$

where u and v are the independent parameters, such that $0 \leq u, v \leq 1$, and $\vec{a}_{k\ell}$ are the polynomial coefficients. Note that the vector coefficient $\vec{a}_{k\ell}$ consists of three elements, one for each of the x, y, and z coordinates. The sixteen vector coefficients can be determined by specifying $\vec{x}, \vec{x}_u, \vec{x}_v$ and $\vec{x}_{uv}$ at four corner points or nodes. (The subscripts u,v refer to the partial derivatives $\frac{\partial}{\partial u}$ and $\frac{\partial}{\partial v}$, respectively.)

The entire surface is defined by a rectangular array of patches. Every four adjacent patches share one common interior corner point or interior node. Around the periphery, every two adjacent patches share one common boundary point or boundary node, except that the corner nodes belong only to the corner patches. This array of patches will be referred to as a network. An illustration is shown in Figure 5.

In Figure 5(a), the geometry for a network of m x n patches is shown in the parametric space. A total of (m + 1)(n + 1) nodes result. The interior nodes are those with index i = 2,3,...,m and j = 2,3,...,n. The others are boundary nodes. Each parameter changes from 0 to 1 within a patch, and the coordinates of the parametric space shown, u' and v', are the cumulative values of the u, v. The boundaries are lines of constant u or v parameters. Normal to the u = constant boundaries, are the tangent vectors $\vec{x}_u$ for each node; and normal to the v = constant boundaries, are the tangent vectors $\vec{x}_v$, parallel to the v = constant and u = constant lines respectively. These tangent vectors required must be specified according to considerations to be discussed in Chapter 4.

The transformation in equation (1) takes a point in the parametric space to a corresponding point in the physical space. It is necessary to determine the remaining 2m + 2n - 4 tangent vectors at the boundary nodes, plus 2(m-1)(n-1)
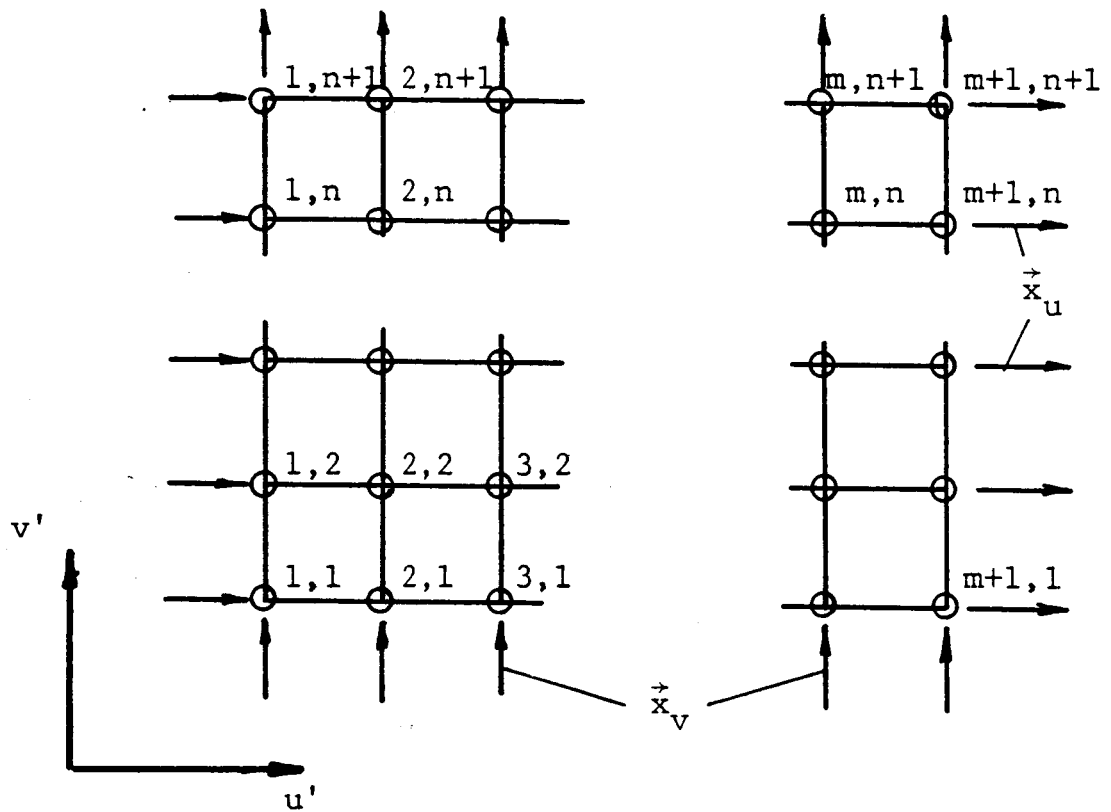
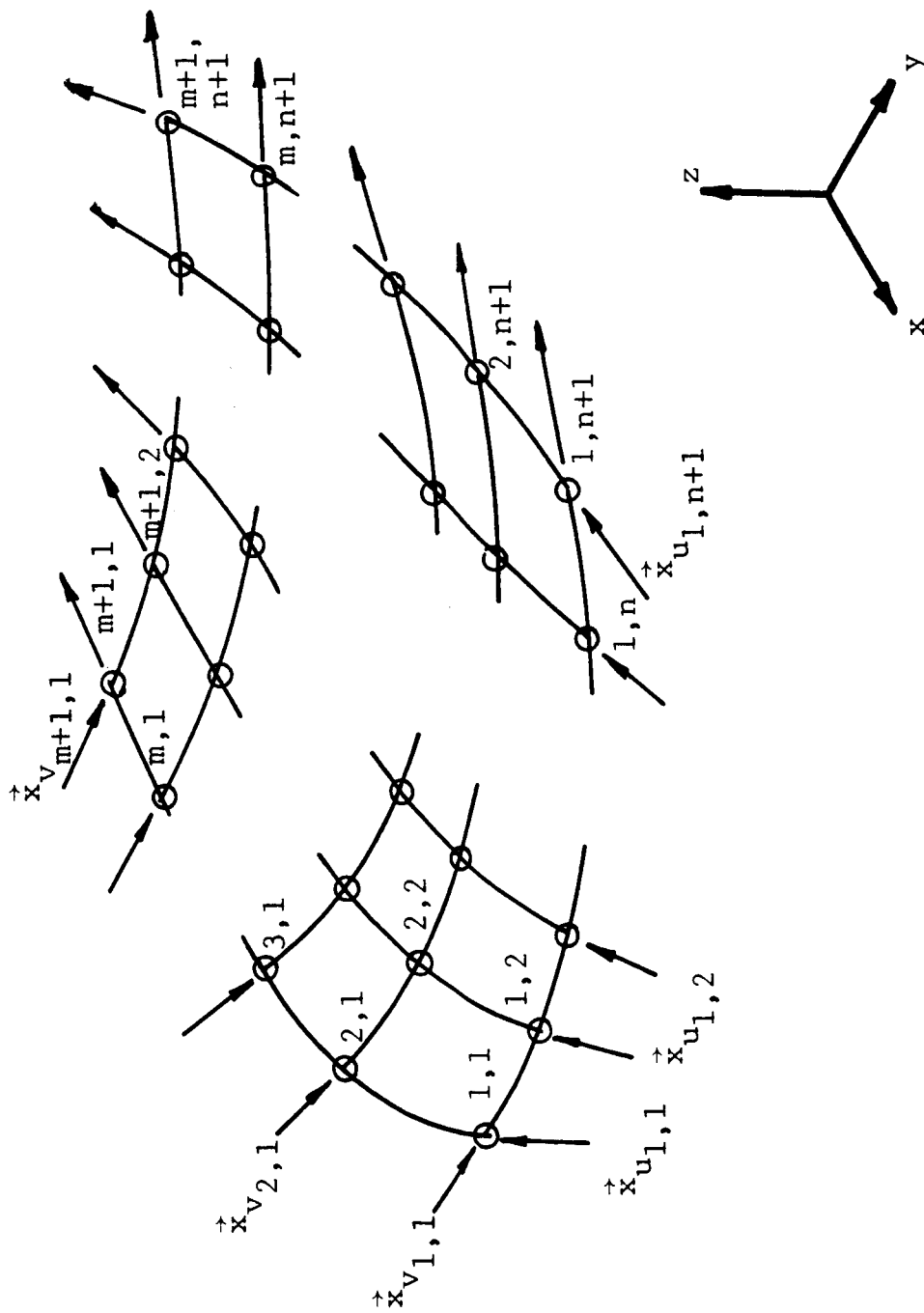Figure 5a.   Patch network geometry in parametric
space

Figure 5b. Patch network geometry in physical space

tangent vectors at the interior nodes. This tangent vector information, together with node coordinates, is sufficient to enable the computation of the sixteen vector coefficients, $[\vec{a}_{k\ell}]$ (in matrix form) according to the matrix relations:

$$[\vec{a}_{k\ell}] = QXQ^T \tag{2}$$

where $X = \begin{bmatrix} x_{00} & x_{01} & x_{v00} & x_{v01} \\ x_{10} & x_{11} & x_{v10} & x_{v11} \\ x_{u00} & x_{u01} & x_{uv00} & x_{uv01} \\ x_{u10} & x_{u11} & x_{uv10} & x_{uv11} \end{bmatrix}$

and $Q = \begin{bmatrix} 1 & 0 & 0 & 0 \\ 0 & 0 & 1 & 0 \\ -3 & 3 & -2 & -1 \\ 2 & -2 & 1 & 1 \end{bmatrix}$

The matrices for the y and z coordinates are similar (12).

The letter subscripts indicate partial differentiation, and the numerical ones indicate the value of the parameter at the patch nodes: the first for u and the second for v. For instance, x_{u01} refers to $\frac{\partial x}{\partial u}$ (u=0, v=1).

Advantages of parametric bicubic patch panels

The main advantage of a higher order patch geometry for an aerodynamic singularity panel resides in its curvature. A much larger number of flat panels is required to obtain the same error in position. For instance, the cubic representa-

tion of a 90° circular arc results in a radial error of $\pm 0.13\%$ of the true circle using one curve segment (12). To obtain the same accuracy with straight segments, eleven would be required.

The cubic requirement is necessary to allow for second derivative continuity and inflection points (12) which are inherent characteristics of the nature of the vortex sheet. In addition, the parametric bicubic is widely used in aircraft design, (3, 18), and its technology is well-established.

The fact that the vortex sheet surface changes directions on itself in the spanwise direction to result in the spiral-like shape, renders explicit functions cumbersome to use. Implicit functions are equally cumbersome since they would require solutions of nonlinear equations at each point. The parametric representation eliminates these difficulties, and moreover handles vertical slopes without special provisions.

Computations of the interior tangent vectors

With reference to Figure 5(b), consider the set of nodes (i,j) with a fixed value of i, i', that is, the nodes $(i',1)$, $(i',2)$, ..., $(i',n+1)$. The patch edges passing through these nodes constitute a space curve, which is a composite parametric cubic which must possess the C^2 property, if the entire surface is C^2. In the case of any i' curve, we obtain a curve whose parameter is v. Similarly, another set of curves, j',

are obtained by varying the parameter u. By differentiating the equation for a curve with constant v:

$$\vec{x}(u) = \sum_{k=0}^{3} a_k u^k \qquad (3)$$

$$\vec{x}_u(u) = \sum_{k=1} k a_k u^{k-1} \qquad (4)$$

$$\vec{x}_{uu}(u) = \sum_{k=2}^{3} k(k-1) a_k u^{k-2} \qquad (5)$$

The requirement is that at the junction of the ith and (i+1)th segments:

$$\vec{x}^i(1) = \vec{x}^{i+1}(0)$$

$$\vec{x}_u^i(1) = \vec{x}_u^{i+1}(0) \qquad (6)$$

$$\vec{x}_{uu}^i(1) = \vec{x}_{uu}^{i+1}(0)$$

Equation (6) must be satisfied to achieve second order continu-

Now, as for the patches in Equation (2), the curve polynomial coefficients can be written in terms of the position and tangent vectors at the nodes:

gent vectors at the nodes:

$$a_0 = r_0$$
$$a_1 = r_{u0}$$
$$a_2 = 3(r_1 - r_0) - 2r_{u0} - r_{u1} \qquad (7)$$
$$a_3 = 2(r_0 - r_1) + r_{u0} + r_u$$

Substituting these values in equation (5), then in the third

of Equation (6),

$$6\vec{x}_0{}^i - 6\vec{x}_1{}^i + 2\vec{x}_{u0}^i + 4\vec{x}_{u1}^i = 6\vec{x}_1^{i+1} - 6\vec{x}_0^{i+1} - 4\vec{x}_{u0}^{i+1} - 2\vec{x}_{u1}^{i+1}$$

But, due to the first two of Equation (6),

$$\vec{x}_{u0}^i + 4\vec{x}_{u0}^{i+1} + \vec{x}_{u1}^{i+1} = 3(\vec{x}_1^{i+1} - \vec{x}_0^i)$$

Now, $\vec{x}_0^i$ refers to node i, $\vec{x}_0^{i+1} = \vec{x}_1^i$ refers to node i + 1 and $\vec{x}_1^{i+1}$ refers to node i + 2. Thus for nodes 2, 3, ..., m, the system of equations results:

$$\vec{x}_u^i + 4\vec{x}_u^{i+1} + \vec{x}_u^{i+2} = 3(\vec{x}^{i+2} - \vec{x}^i) \qquad i=1,2,\ldots,m-1 \qquad (8)$$

where i here denotes the ith node rather than patch as done earlier.

If $\vec{x}_u^1$ and $\vec{x}_u^{m+1}$ are known, then the remaining m-1 tangent vectors at the interior nodes can be found efficiently by solving the above tridiagonal system by the Thomas' algorithm, (1).

The above is repeated for all n+1 curves, then, in the transverse direction, for all m+1 curves in a similar fashion.

The remaining derivatives $\vec{x}_{uv}$, also called the cross derivatives, or twist vectors, have zero values along lines of minimum or maximum surface curvature. For simplicity, this assumption was made and, as indicated by (12), results in a negligible amount of error.

In the same reference, it is shown that the patches are continuous in C^2 across their common boundaries if the above curve continuity is achieved.

Geometric Properties of Interest

The main purpose of a patch is to serve as a surface position interpolant, i.e., given a parameter pair of values, a corresponding set of physical coordinates of a point on the surface of patch i is obtained:

$$\vec{x} \equiv (x, y, z) = \sum_{k=0}^{3} \sum_{\ell=0}^{3} \vec{a}_{k\ell}^{i} u^k v^{\ell} \tag{9}$$

such that $0 \leq u, v \leq 1$.

In addition, a tangent vector to the surface at the point is a linear combination of a pair of tangent vectors, $\vec{x}_u = \frac{\partial \vec{x}}{\partial u}$ and $x_v = \frac{\partial \vec{x}}{\partial v}$ which are obtained merely by differentiating with respect to the parameters u or v. If $\vec{x}_u \neq \alpha \vec{x}_v$, where α is a scalar, then the vector product $\vec{x}_u \times \vec{x}_v$ is a vector normal to the surface at the given point.

<u>Elemental area</u>   As illustrated in Figure 6, the elemental area dA is given by:

$$dA = |\vec{x}_u du| \cdot |\vec{x}_v dv| \sin \theta = |\vec{x}_u \times \vec{x}_v| dudv$$

$$= |\hat{i}(y_u z_v - y_v z_u) + \hat{j}(x_v z_u - x_u z_v) + \hat{k}(x_u y_v - x_v y_u)| dudv$$

where $\hat{i}, \hat{j}, \hat{k}$ are the unit vectors in the x,y,z directions.
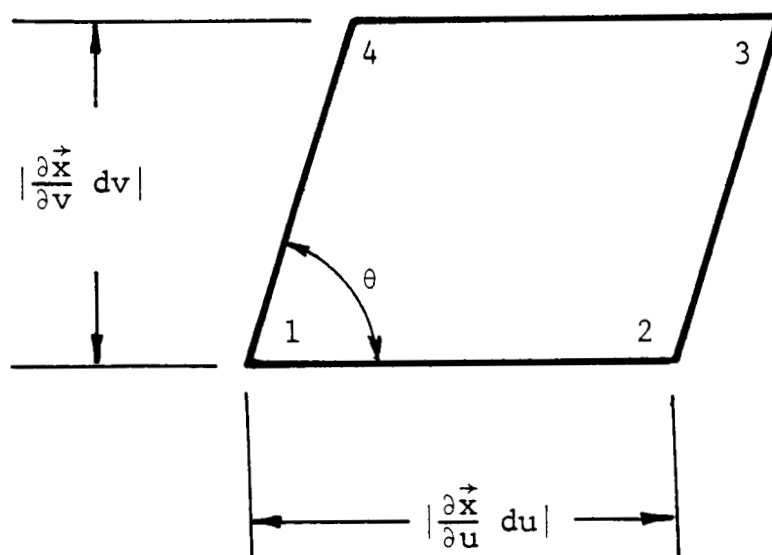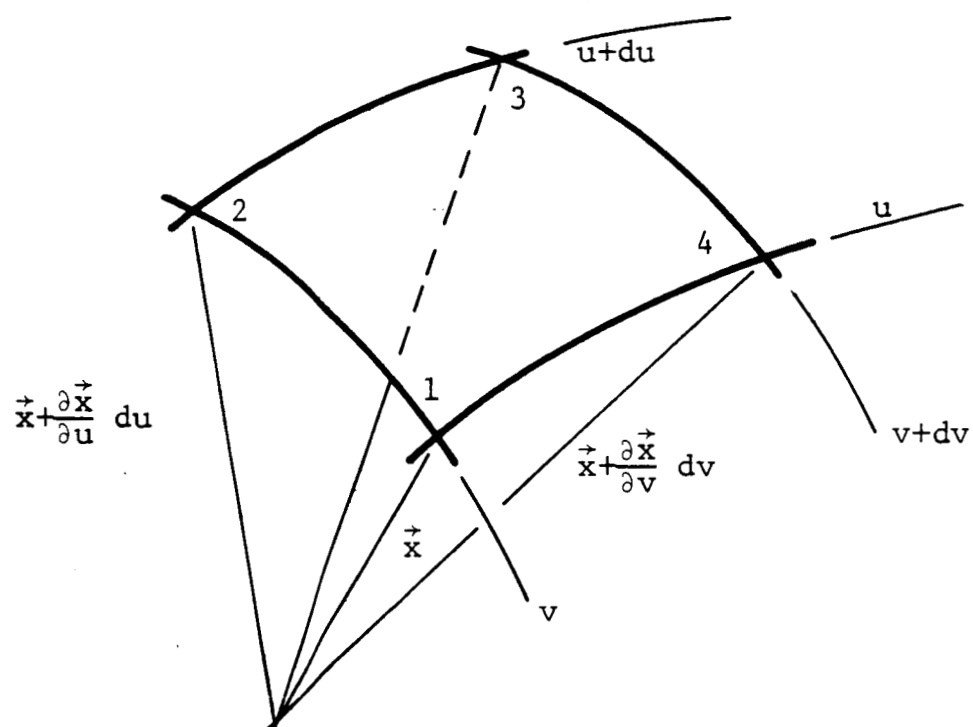
Figure 6.   Elemental area on a patch

Integration of a function over the surface of a patch

It will be necessary to integrate the induced effects of the vorticity which is distributed over the patch area, and expressed as a function f of u and v. To evaluate the integral

$$I = \iint_{S} f(u,v)\,dA, \tag{10}$$

where S is the boundary surface bound in one patch, and dA is the elemental area, the relation above is used, thus

$$I = \int_{0}^{1}\int_{0}^{1} f(u,v)\,|\vec{x}_{u} \times \vec{x}_{v}|\,du\,dv. \tag{11}$$

CHAPTER III: SINGULARITY SOLUTIONS FOR POTENTIAL FLOW
Governing Equations and Solutions

For steady, irrotational motion of an inviscid perfect
fluid, the velocity perturbation potential function satisfies
the Prandtl-Glauert equation:

$$(1-M_\infty^2) \; \phi_{xx} + \phi_{yy} + \phi_{zz} = 0$$

which is valid for small perturbations, but not for transonic
flow.   For <u>subsonic</u> flow, by replacing x by $x(1-M^2)^{-\frac{1}{2}}$, the
equation reduces to Laplace's equation:

$$\nabla^2 \phi = \phi_{xx} + \phi_{yy} + \phi_{zz} = 0$$

This equation also holds for incompressible irrotational flow
in general.

Applying Green's theorem, it can be shown (2) that
Laplace's equation can be converted to the integral equation:

$$\phi_P = \frac{1}{4\pi} \iint_S [-\frac{\partial \phi}{\partial n} \cdot \frac{1}{r} + \phi \cdot \frac{\partial}{\partial n}(\frac{1}{r})] dS \tag{12}$$

where: P is a point in the flow field domain $\mathcal{D}$,

   S is the boundary of $\mathcal{D}$,

   n is the unit vector normal to S at a point Q on the
   surface, and

   r is the distance from P to Q.   (Refer to Figure 7.)
This equation is a singularity solution to Laplace's equation.
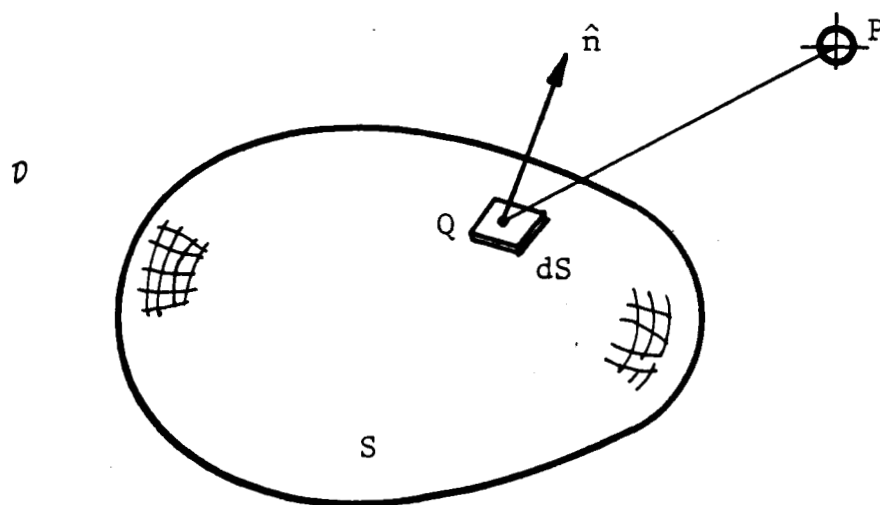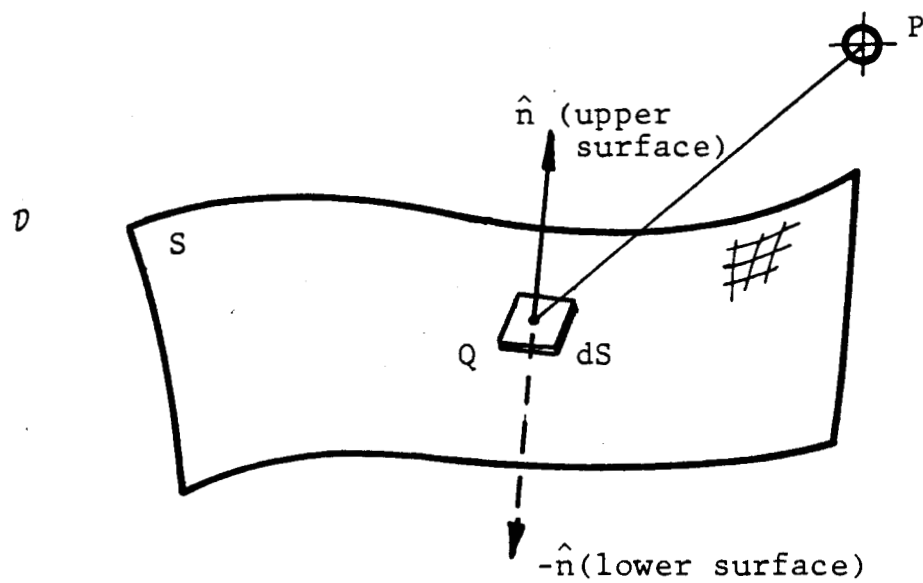
Figure 7a. Boundary for a closed surface.

Figure 7b. Boundary for an open surface

The two terms in the integrand contain

$$\frac{-1}{4\pi r} \quad \text{and} \quad \frac{\partial}{\partial n}(\frac{1}{4\pi r})$$

which are the potential functions of a point source and a doublet, respectively. The terms ϕ and $\frac{\partial \phi}{\partial n}$ represent the source and doublet strengths at point Q, thus equation (12) can be rewritten as:

$$\phi(\vec{\xi}) = \frac{1}{4\pi} \iint [\frac{-\sigma(\vec{x})}{|\vec{\xi}-\vec{x}|} + \mu(\vec{x})\frac{\partial}{\partial n}(\frac{1}{|\vec{\xi}-\vec{x}|})] dS \qquad (13)$$

where: $\vec{\xi}$ is the position vector of field point P,

$\vec{x}$ is the position vector of boundary point Q,

$\sigma(\vec{x})$ source strength distribution on the boundary S,

and $\mu(\vec{x})$ doublet strength distribution on the boundary S.

In panel methods, σ and μ are approximated by piecewise constant, linear or quadratic distributions over each surface finite element, called a panel, so that for K panels:

$$\phi(\vec{\xi}) = \sum_{i=1}^{K} \{\frac{1}{4\pi} \iint_{S_i} [\frac{-\sigma i}{r} + \mu_i \frac{\partial}{\partial n} \frac{1}{r}] dS\} \qquad (14)$$

where S_i is the area of the ith panel. By properly specifying boundary conditions at a number of points (K), called control points, selected in this case on the surface, a set of simultaneous linear equations can be obtained and solved for σ_i, μ_i.

Usually, source panels are used for closed surfaces and

solid boundaries, while doublet panels are used for thin lifting surfaces, or for lift generation on solid boundaries as well as for barriers such as vortex sheets to render $\mathcal{D}$ simply connected.

In this study, only the doublet solution will be of concern, even though source distributions may be included to represent solid boundaries and their effect on the roll-up process of the vortex sheet.

Higher Order Doublet Panels

Unlike the panel method techniques where the objective is to solve for the singularity strengths, in the present case, the wing lift distribution, a function of the spanwise location, is known *a priori*. It could be determined for a given configuration from some panel method computer code, experimentally, or by some other means. The problem here is to determine the induced effects of the vorticity at various key points of the flow field, in order to determine displacements and thus modify the shape of the vortex sheet. Constant doublet strength panels are equivalent to discrete ring vortices, and a substantial approximation results. In the interest of maintaining adequate accuracy without an excessive number of panels of constant doublet strength, a bilinear or biquadratic doublet distribution is used.

Bilinear:

$$\mu_I(u,v) = \mu_1 + \mu_2 u + \mu_3 v + \mu_4 uv \tag{15}$$

Biquadratic:

$$\mu_{II}(u,v) = \mu_I(u,v) + \mu_5 u^2 + \mu_6 v^2 + \mu_7 u^2 v + \mu_8 uv^2 + \mu_9 u^2 v^2$$

where u and v are the arc length in the streamwise and span-wise directions, respectively, of the vortex sheet.

In the free portion of the vortex sheet, the doublet strength does not vary streamwise, and u is a constant there.

Equivalence of doublet and vortex panels

The induced velocity at a point P due to an elemental vortex panel of area dS is obtained from the Biot-Savart law:

$$d\vec{V}_v = \frac{\hat{t} \times \vec{r}}{|\vec{r}|^3} \gamma dS \tag{16}$$

where: $\vec{r}$ is the relative position vector of P with respect

to the panel centroid.

$\hat{t}$ is a unit vector in the direction of the vorticity.

γ is the local vorticity strength.

The velocity potential at a point P due to a doublet panel of local strength μ with normal vector $\hat{n}$ is:

$$d\phi_D = \frac{\vec{r} \cdot \hat{n}}{|\vec{r}|^3} \mu dS$$

It can be shown that $\gamma \cdot \hat{t}$ is equivalent to $\hat{n} \times \nabla\mu$, (16), thus producing the same potential function in D.   Both

approaches are used. In reference (27), the doublet panel
is preferred because the doublet strength is a scalar.
However, a biquadratic approximation is used to reduce the
approximation error, since the first order error term is
nonexistent, resulting in a more complex panel model.
Reference (18) suggests the use of a bilinear vorticity
distribution, which is an equivalent approximation to the
biquadratic doublet panel.

To assess the approximation error, consider a two-
dimensional flat vortex sheet as in Figure 8. The induced
vertical velocity at point x on the sheet segment from $x_1=0$
to $x_1=c$ is given by:

$$V_z(x,0) = \frac{1}{2\pi} \int_0^c \frac{\gamma(x_1)dx_1}{x_1 - x} \tag{17}$$

Expanding $\gamma(x_1)$ in Taylors' series about x:

$$\gamma(x_1) = \gamma(x) + \frac{d\gamma}{dx}(x)\cdot(x_1-x) + \frac{1}{2}\frac{d^2\gamma}{dx^2}(x)(x_1-x)^2 + \ldots$$

Substituting in Equation (17):

$$V_z(x,0) = \frac{1}{2\pi} \int_0^c [\frac{\gamma(x)}{x_1-x} + \frac{d\gamma}{dx}(x) + \frac{1}{2}\frac{d^2\gamma}{dx^2}(x)(x_1-x) + 0^2(x_1-x)]dx_1$$

$$= \frac{1}{2\pi}[\gamma(x) \int_0^c \frac{dx_1}{x_1-x} + \frac{d\gamma}{dx}(x)\cdot c + \frac{1}{2}\frac{d^2\gamma}{dx^2}(x) \int_0^c (x_1-x)dx_1] + \frac{1}{2\pi}0^2(x_1-x).$$
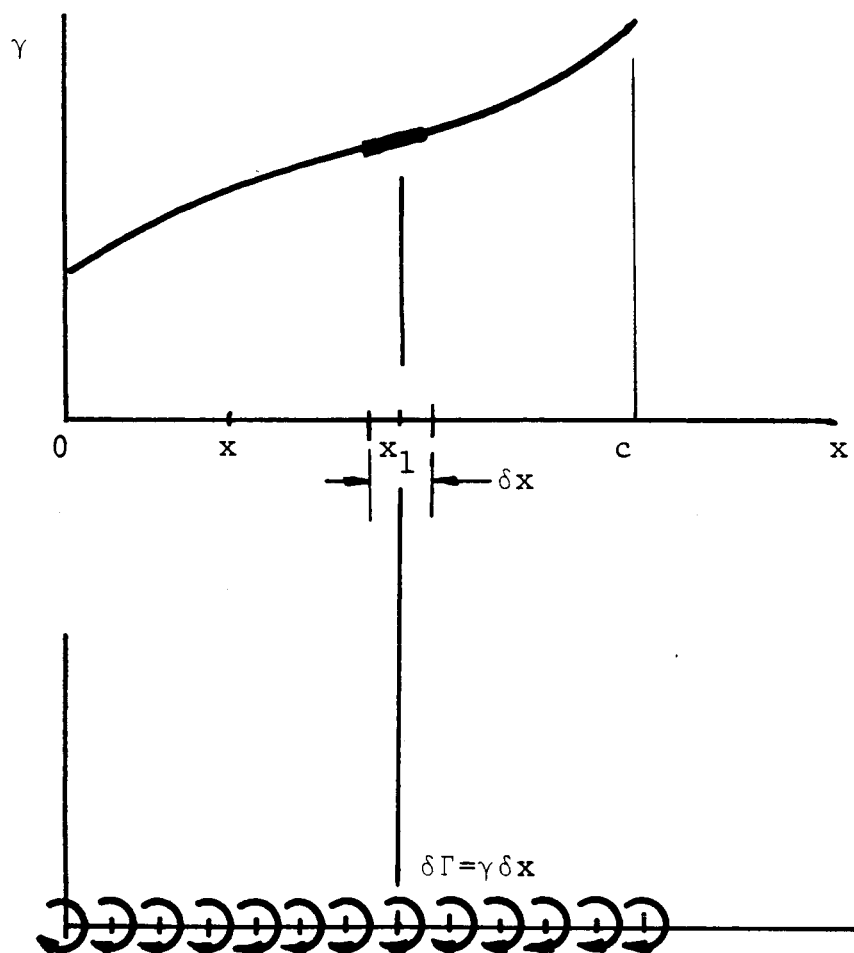
Figure 8. Vorticity distribution on a two-dimensional flat surface along the x-axis

If point x is the midpoint of a panel, the first and third terms in the square brackets vanish. Thus, in order not to exceed second order error, the derivative $\frac{d\gamma}{dx}$ must be nonzero. This is achieved by using a bilinear γ distribution. Biquadratic distribution will not reduce the error. In addition, since the bilinear distribution over each panel provides C^0 (continuity of value) for γ, there will be no concentrated vorticity at the panel edges.

Analysis similar to the above can be used to demonstrate that source panels possess the same behavior, and bilinear source distributions would result in a second order error in the distance from the control point.

Derivation of the vortex panel induced velocity for the free vorticity

Considering the geometry of one panel represented by a parametric bicubic, the vorticity vectors are tangential to lines of constant values of the parameter v, which are space curves lying in the vortex sheet, oriented in the general streamwise directions as shown in Figure 9. By virtue of Helmholtz' first vortex theorem, the strength will not vary along these curves. Therefore, each v-line is a vortex filament of infinitesimal strength $\gamma(y_1)dy_1$, where y_1 is the y-coordinate of the generating wing trailing edge. As indicated earlier, $\gamma = \gamma(y_1)$ is known. For simplicity, it will be approximated by a piecewise linear distribution in v
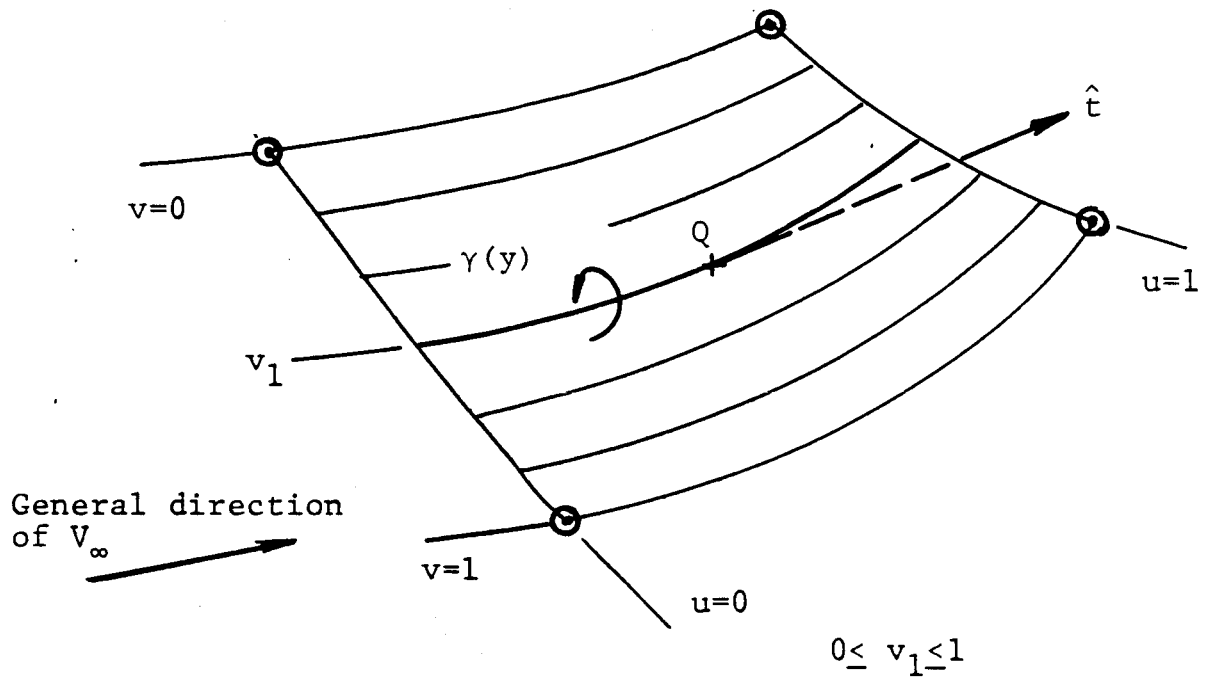
Figure 9. Vortex panel configuration for vorticity
along a $v=v_1$ curve

between the nodes of the free vortex sheet's leading edge, which coincides with the wing's trailing edge. For the panels with index j,

$$\gamma(v) = \gamma(y_{j-1}) + [\gamma(y_j) - \gamma(y_{j-1})]v \qquad (18)$$

at any point on such panel whose position vector $\vec{x}$ is given by Eq. (1). The unit tangent vector is given by

$$\hat{t} = \frac{\vec{x}_u}{|\vec{x}_u|} \qquad (19)$$

The vorticity induced velocity at a point whose position vector is $\vec{\xi}$ due to the vorticity in panel i,j is obtained by integrating Eq. (16) using Eq. (11):

$$\vec{v}^{i,j} = \frac{1}{4\pi} \int_0^1\int_0^1 \frac{\vec{x}_u \times (\vec{\xi}-\vec{x})}{|\vec{x}_u||\vec{\xi}-\vec{x}|^3} \gamma(v) |\vec{x}_u \times \vec{x}_v| \, dudv \qquad (20)$$

with m × n is the number of patches representing the sheet in the stream- and spanwise directions, respectively.

Derivation of the vortex panel induced velocity for the bound vorticity

The formulation is identical to that of the free vorticity with the exception that the vector $\hat{t}$ does not coincide with $\vec{x}_u$, but is a linear combination of $\vec{x}_u$ and $\vec{x}_v$. Equation (20) is thus applicable to the component along $\vec{x}_u$ inducing V_1. The other component along $\vec{x}_v$ induces a velocity vector V_2:

$$\vec{V}_1^{i,j} = \frac{1}{4\pi} \int_0^1\int_0^1 \frac{\vec{x}_u \times (\vec{\xi}-\vec{x})}{|\vec{x}_u||\vec{\xi}-\vec{x}|^3} \, \gamma_1(u,v)|\vec{x}_u \times \vec{x}_v|\,dudv \qquad (21a)$$

$$\vec{V}_2^{i,j} = \frac{1}{4\pi} \int_0^1\int_0^1 \frac{\vec{x}_v \times (\vec{\xi}-\vec{x})}{|\vec{x}_v||\vec{\xi}-\vec{x}|^3} \, \gamma_2(u,v)|\vec{x}_u \times \vec{x}_v|\,dudv \qquad (21b)$$

also,

$$\vec{V}^{i,j} = \vec{V}_1^{i,j} + \vec{V}_2^{i,j}$$

and for the entire sheet consisting of mxn panels:

$$\vec{V} = \sum_{i-1}^{m} \sum_{j=1}^{n} \vec{V}^{i,j} \qquad (22)$$

CHAPTER IV: THE VORTEX SHEET
Review of Methods of Rollup Prediction

<u>Betz' Theory</u>

The earliest attempt to analyze the behavior of vortex systems in a manner applicable to the prediction of the then known phenomenon of vortex sheet rollup was introduced by Betz in 1932 (4). The theory is based on the Kutta-Joukowsky theorem of vortex lift on a body L, about which a circulation Γ exists:

$$L = \rho V \Gamma$$

where ρ is the fluid density, and V is the linear velocity of the body relative to the fluid perpendicular to L. Thus, if a system of such bodies interact, with the bodies becoming infinitely small, and if there are no solid outer boundaries to exert a force, the net lift forces and moments of these interacting vortices must be zero. As a consequence, and as a consequence of Helmholz' theorem, the following conservation rules can be written to relate the vorticity in the sheet as it leaves the wing trailing edge, with that of the rolled-up sheet:

1. Vorticity:

$$\int_y^{b/2} \frac{d\Gamma(y)}{dy}\, dy = \int_r^R \frac{d\Gamma(r)}{dr}\, dr \tag{23}$$

The left-hand side of the equation refers to the initial flat sheet at the wing trailing edge, y being any spanwise station and b the wing span. The right-hand side refers to the rolled-up vortex core, r being a radial position in the vortex core from its center and R the core radius.

2. The first moment of vorticity:

$$-\int_{y}^{b/2} \frac{d\Gamma(y)}{dy} \, ydy = \int_{r}^{R} \frac{d\Gamma(r)}{dr} \, rdr \qquad (24)$$

As a consequence, the centroid of the vorticity located at :

$$\bar{y} = -\frac{1}{\Gamma_0} \int_{y}^{b/2} \frac{d\Gamma(y)}{dy} \, ydy$$

where

$$\Gamma_0 = \int_{y}^{b/2} \frac{d\Gamma(y)}{dy} \, dy$$

remains at a constant spanwise station. The vertical position, however, will change since there is an external force, the wing lift, applied to the fluid elements which results in a downward motion of the centroid.

3. The second moment of vorticity about the centroid:

$$\int_{y}^{b/2} \frac{d\Gamma(y)}{dy} (y-\bar{y})^2 \, dy = \int_{r}^{R} \frac{d\Gamma(r)}{dr} r^2 dr \qquad (25)$$

These relations can be used to determine the structure of the rolled-up vortex core, that is, the position of the core radius r in which a portion of the sheet from a station y to the tip is contained. Rossow (25) shows that

$$r = \bar{y} - y$$

Wings with nonsimple loading, such as for flaps extended configurations can also be treated using a method developed in reference (8).

Unfortunately, these rules and methods are helpful only for fully developed vortex cores, since the time history of the rollup cannot be predicted.

Time History of Rollup

In 1935, Westwater (32) developed a technique for obtaining the vortex sheet shape by representing it with discrete vortices of finite strength and infinite length, and computing their positions at successive time increments. These positions are equivalent to flow streamlines and the time increments correspond to streamwise stations. Computations are performed in the Trefftz Plane, that is, the infinite filaments are assumed straight and perpendicular to the plane. The bound vorticity is ignored and thus the problem is reduced to two-dimensions. The induced velocity at a point where any one

vortex filament intersects the Trefftz Plane is the sum of the induced velocity vectors of each vortex filament except the one in question. The point is moved by an incremental displacement equal to the time increment times the induced velocity vector. This is done for each filament and the process repeated for various streamwise stations to obtain the time history of the configuration. Plots of Westwater's results are given in his paper as well as in (30) and (9) for an elliptic loading using 20 filaments for the entire span.

Discretization seems to lead to several problems. The elimination of the filament at which the induced effects are being computed is both valid and necessary for a finite or discrete system, however, it is a poor representation of a continuous system since it creates a "gap" in the sheet. Should the number of filaments be increased, the two vortices adjacent to the point in question would become too close and result in excessive induced velocities. Another problem is the increased strength of the tip filaments, compared to the remaining ones. Moore has found, as reported by El-Ramly (9), that such tip filaments will circle around each other, implying that the sheet intersects itself.

Some of these idealizations were removed by Butter and Hancock (6). Three-dimensional effects were considered. A line vortex at the quarter chord was introduced to represent

bound vorticity, and the trailing vorticity is only semi-infinite. A similar effort was conducted by Hackett and Evans (14). The discretization effects are the same as above.

Reference (9) notes the work of Neilsen and Schwind, where some treatment is done to alleviate the discretization effects, namely, when two vortices come too close to each other, they are combined into one at their centroid.

Other researchers whose works are surveyed by El-Ramly (9), concentrate on fully rolled up vortex cores, the distances for full roll-up and other related parameters not directly related to the present study, for both inviscid and viscous solutions. The inclusion of viscous effects to predict decay of vorticity and the merging of co-rotating cores has received considerable attention in the '70s decade when the wake hazard of large aircraft became manifest. Again, these works are surveyed in (9, 23). Experimental work was conducted at Iowa State University (reference 19), to study the merging of vortex cores which are fully developed. There, two separate wings were used to generate a pair of rolled-up vortex cores, in order to simulate multiple cores generated by a single wing of a large aircraft during climb or approach near airports, where the wake hazard is serious. The merging of such cores may be desirable since it can lead to vortex cores with diffused vorticity representing a reduced hazard

to trailing aircraft. Much of the research (9, 24) deals

with the injection of auxiliary vortices which merge with

the primary tip vortex, as well as methods of assuring

speedy decay. For a specific aircraft configuration, it

is helpful to know where such cores will be situated upon

completion of rollup, and the relative magnitudes of their

strengths. Then, analytical or experimental predictions of

merging and decay can be simplified.

The present method in essence is similar to that of

Butter and Hancock (6), but removes many restricitons which

lead to over-simplifications. Mainly, a continuous distribu-

tion of vorticity, truly three-dimensional effects of the

vortex sheet shape, and a lifting surface are used with the

help of the building blocks described in Chapters II and III.

Furthermore, the technique is compatible with the advanced

aerodynamic paneling techniques in use today, allowing ready

incorporation of rollup effects, if desired.

The remainder of this chapter describes the method used

from the physical and computational standpoint.

Sheet Vorticity Strength Distribution

Panel Vorticity

At any point P on the vortex sheet (see Figure 10), the

vorticity strength vector $\vec{\gamma}$ can be resolved in two components

$\gamma_1 = \frac{\partial \Gamma}{\partial s_1}$ and $\gamma_2 = \frac{\partial \Gamma}{\partial s_2}$, which are tangential to the u=constant and v=constant curves at point P, respectively. Γ is the circulation in the sheet at point P, and s_1 and s_2 are arc lengths in the direction of γ_2 and γ_1, respectively. Note that γ_1 and γ_2 are not necessarily perpendicular to each other. It is necessary to express these vectors in terms of their values at the patch nodes, using a bilinear distribution as indicated earlier. For the magnitude,

$$\gamma(u,v) = u_{11}\gamma_{i,j} + u_{21}\gamma_{i+1,j} + u_{12}\gamma_{i,j+1} + u_{22}\gamma_{i+1,j+1} \quad (26)$$

where,

$\gamma_{i,j}$ are the magnitudes of γ_1 or γ_2 at nodes (i,j),

$u_{11} = 1 - u - v + uv$,

$u_{21} = u - uv$,

$u_{12} = u - uv$, and

$u_{22} = uv$.

For the direction, the unit tangent vectors $\hat{t}_1$, $\hat{t}_2$ are merely the tangents to the v=constant and u=constant curves, respectively, so that:

$$\hat{t}_1 = \vec{x}_u / |x_u| , \text{ and}$$

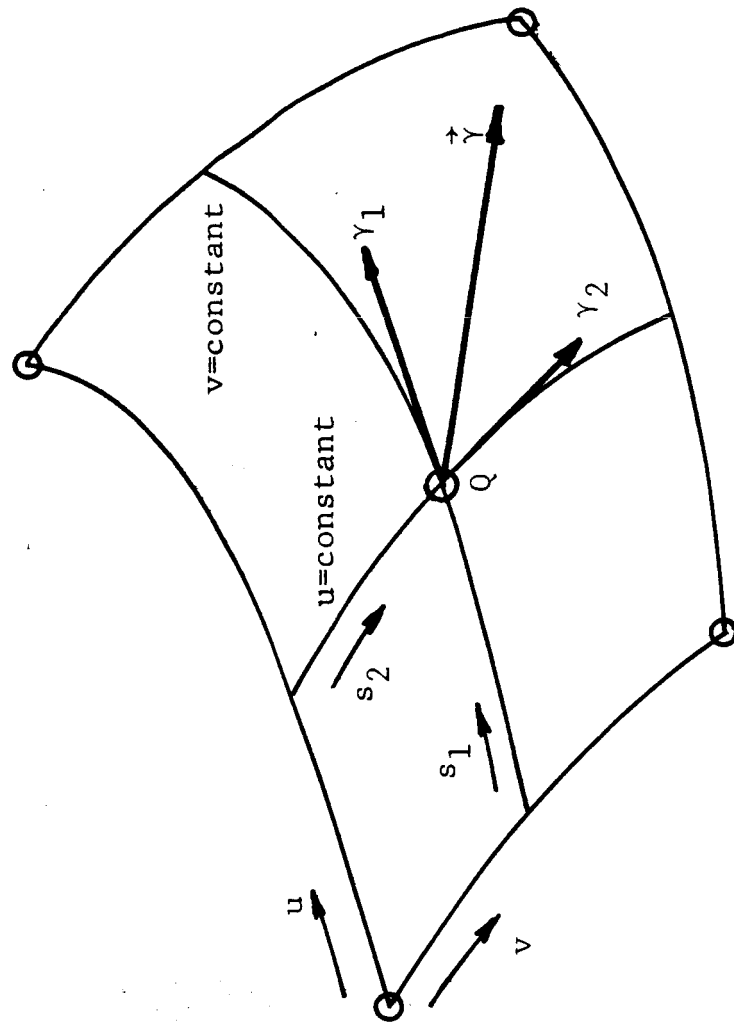$$\hat{t}_2 = \vec{x}_v / |x_v| \quad (27)$$

Figure 10. Panel vorticity

Computation of nodal vorticity strengths

It is assumed here that: (1) the wing spanwise loading and (2) the chordwise loading distributions at various span locations are known. A number of wing stations (span locations) are selected, and the values of $\gamma_1 = \frac{d\Gamma}{dy}$ at these stations obtained, where Γ is the bound vorticity strength at the spanwise station y. The value of Γ is obtained from elementary vortex lift theory (Kutta-Joukowsky):

$$\Gamma = \frac{1}{2} V_\infty C\, C_\ell$$

where C and C_ℓ are the local chord length and lift coefficients, respectively.

Between a pair of consecutive wing stations, j and j+1, γ_1 is approximated by a linear distribution in y:

$$\gamma_1(y) = \frac{(\gamma_1)_{j+1} - (\gamma_1)_j}{y_{j+1} - y_j} (y - y_j) + (\gamma_1)_j$$

The change in bound vorticity strength in this interval, $\Gamma_{j+1} - \Gamma_j$ must be equal to the strength of the shed or trailing vorticity. As a direct result of Helmholtz' first vorticity theorem:

$$\Gamma_{j+1} - \Gamma_j = \int_{y_i}^{y_{j+1}} \gamma_1 dy$$

$$= \frac{y_{i+1} - y_i}{2} [(\gamma_1)_{j+1} + (\gamma_1)_j]$$

Γ_j is distributed in the chordwise direction in a fashion similar to that of the load distribution, $C_{p_\ell} - C_{p_u}$, where C_p is the pressure coefficient, and the subscripts refer to lower or upper surfaces of the wing. Figure 11 depicts typical distributions for two categories of airfoils. In addition, the following relation holds:

$$\Gamma_j = \int_0^{C_j} \gamma_2 dx$$

at any wing station j. γ_2 denotes the component of vorticity proceeding in the spanwise direction. It is again approximated by a piecewise linear distribution (Figure 12), i.e., linear over a chord segment from point i to point i+1.

$$\gamma_2(x) = \frac{(\gamma_2)_{i+1} - (\gamma_2)_i}{x_{i+1} - x_i} (x - x_i) + (\gamma_2)_i$$

Between two consecutive stations j, j+1, a linear blending function is used to interpolate, and thus the bilinear distribution is used. The same interpolation method is used for γ_1.

Now, since $\Gamma_j = \int_0^C \gamma_2 dx$, the piecewise interpolant results in a trapezoidal rule summation:

$$\Gamma_j = \sum_{i=1}^{m} \frac{x_{i+1} - x_i}{2} [(\gamma_2)_{i+1} + (\gamma_2)_i]$$
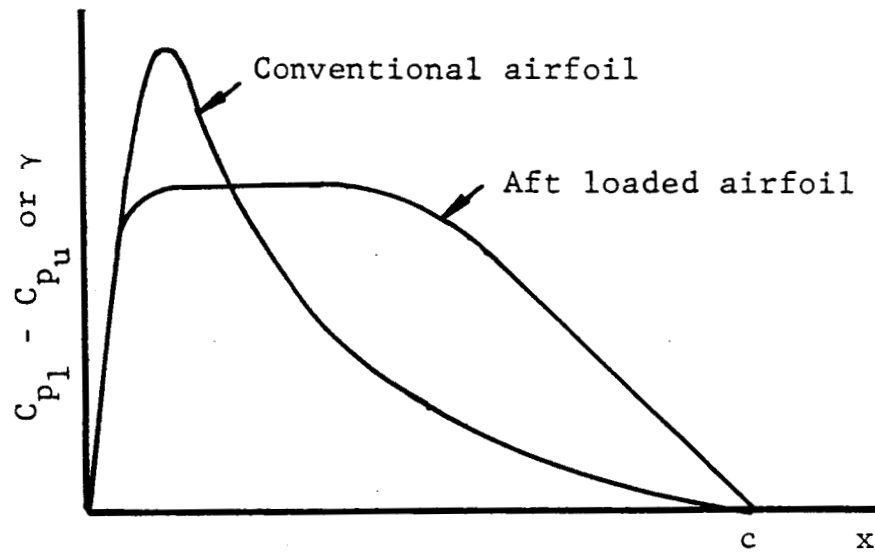
Figure 11a.   Typical chordwise vortex strength
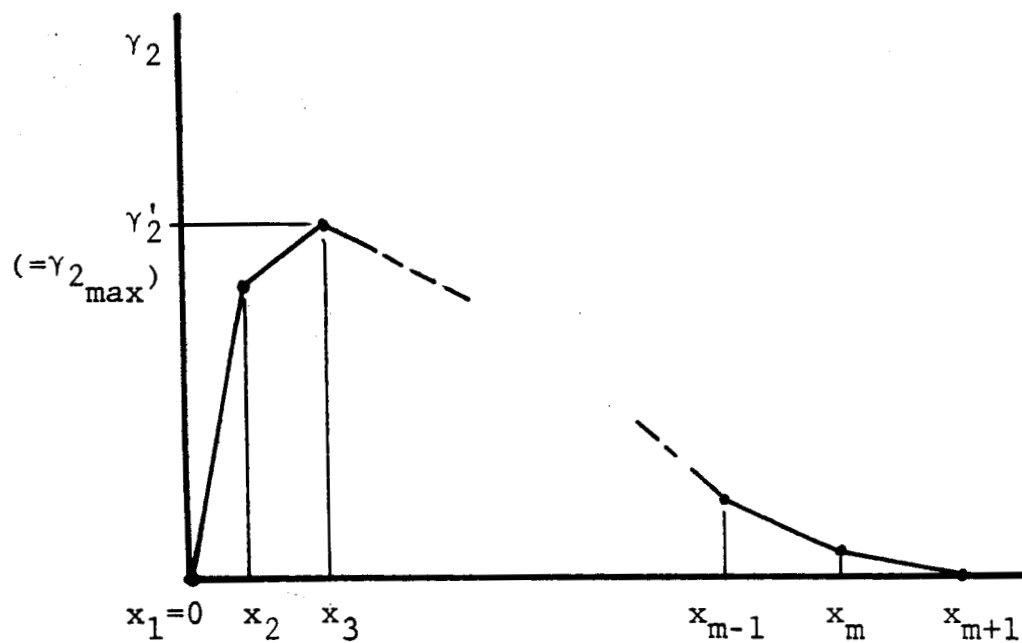distributions

Figure 11b.   Approximation of chordwise loading
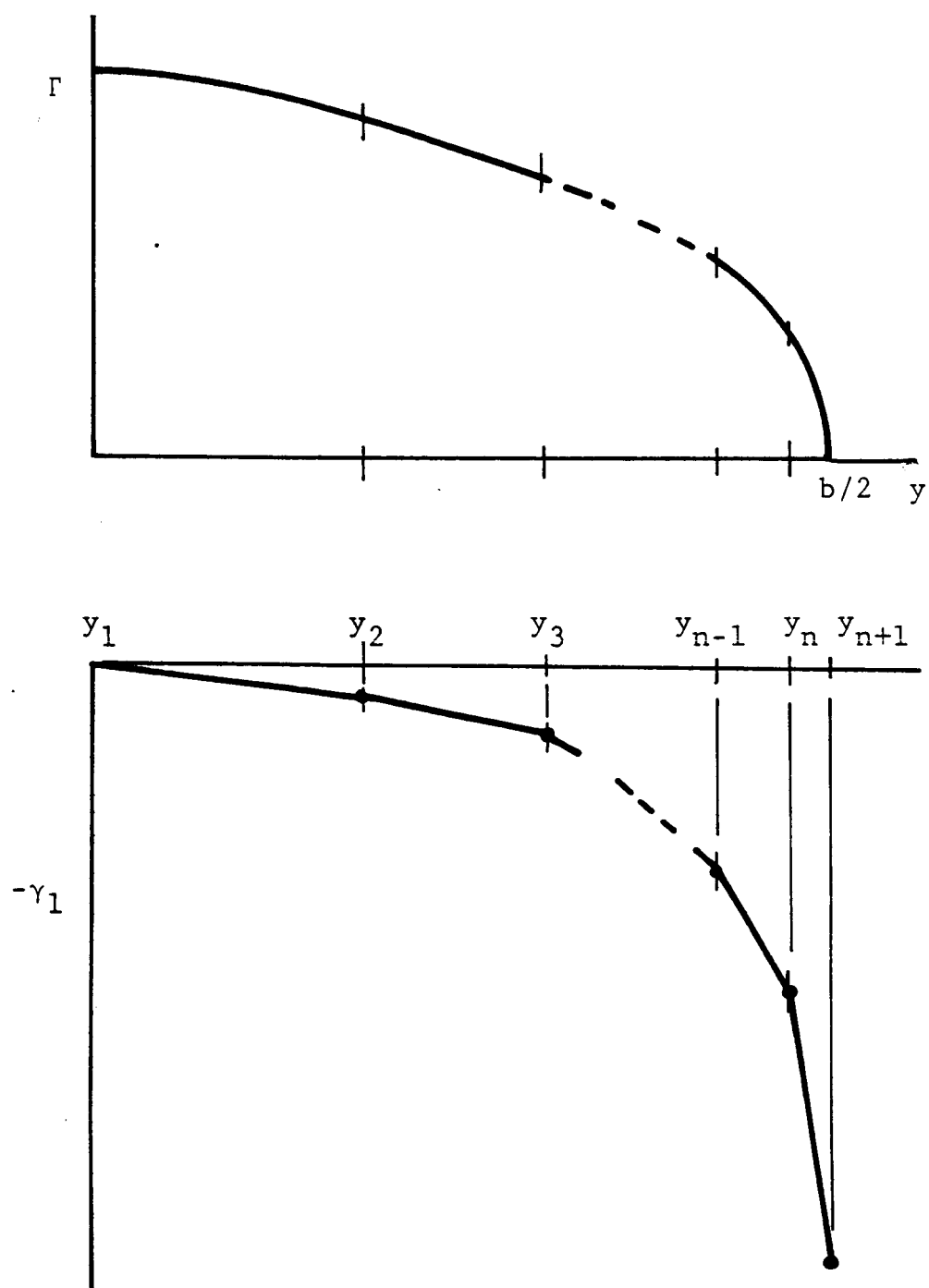distribution using a linear
interpolant

Figure 12. Typical spanwise load distribution for a wing and piecewise linear approximation of corresponding shed vorticity

Since the distribution is known, the $(\gamma_2)_i$ can be expressed as multiples of γ_2', the maximum γ_2 value along the chord, then

$$\Gamma_j = \frac{1}{2} \gamma_2' \sum_{i=1}^{m} [(\tilde{\gamma}_2)_{i+1} + (\tilde{\gamma}_2)_i] \Delta x_i = f \cdot \gamma_2' \qquad (28)$$

or,

$$\gamma_2' = \Gamma_j / f \qquad (29)$$

where:

$$f = \frac{1}{2} \sum_{i=1}^{m} [(\tilde{\gamma}_2)_{i+1} + (\tilde{\gamma}_2)_i] \Delta x_i$$

$$\Delta x_i = x_{i+1} - x_i, \qquad (30)$$

and

$$\tilde{\gamma}_2 = \gamma_2 / \gamma_2'$$

Therefore, the vorticity flow through the panel edge (1), on Figure 13, has the circulation

$$\Gamma_1 = [(\gamma_2)_{i+1} + (\gamma_2)_i]_j \Delta x_i$$

$$= \gamma_2' [(\tilde{\gamma}_2)_{i+1} + (\tilde{\gamma}_2)_i]_j \Delta x_i \qquad (31)$$

and through panel edge (2)

$$\Gamma_2 = [(\gamma_2)_{i+1} + (\gamma_2)_i]_{j+1} \Delta x_i = \gamma_2' [(\tilde{\gamma}_2)_{i+1} + (\tilde{\gamma}_2)_i]_j \Delta x_i \qquad (32)$$
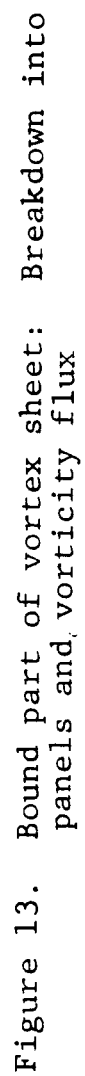
Figure 13. Bound part of vortex sheet: Breakdown into panels and vorticity flux

Similarly, through panel edge (3), the vorticity flow has the circulation:

$$\Gamma_3 = [(\gamma_1)_{j+1} + (\gamma_1)_j]_i \, \Delta y_j \tag{33}$$

and through panel edge (4):

$$\Gamma_4 = [(\gamma_1)_{j+1} + (\gamma_1)_j]_{i+i} \Delta y_j \tag{34}$$

The following conditions must be noted:

1. $\Gamma_1 + \Gamma_3 = \Gamma_2 + \Gamma_4$ $\hspace{2cm}$ (35)

2. $\gamma_1 = \gamma_2 = 0$ $\hspace{3cm}$ (36)

along the leading edge, and

3. $\gamma_1 = 0$ $\hspace{4cm}$ (37)

along the centerline or plane of symmetry.

If Γ is known at the centerline, and γ_1 is known at all wing stations, which are determined *a priori* along with the chordwise loading, then by virtue of Equations 28-30, 36, γ_2' at each station, and thus γ_2 at all nodes can be obtained. By virtue of Equations 31-36, the values of γ_1 at all nodes can be obtained too.

In the free portion of the vortex sheet, the wake $\gamma_2 = 0$ everywhere, and the values of γ_1 remain unchanged from those at the trailing edge.

In the parametric patch representation scheme, all variables are expressed in terms of the parameters u and v,

which are used to represent the streamwise and spanwise directions with proper transformations, respectively.

As a matter of general interest, in the panel methods where the circulation is everywhere unknown, it is customary to express the nodal circulation values in terms of a subset of values, usually one per spanwise station. The induced effects are then added to the source panels representing the solid boundaries. An additional number of equations equal to the number of unknowns (in this case the γ_2' values) is required. These are obtained by specifying boundary conditions at an equal number of points, for example, where the Kutta condition may be enforced. The problem of the vector nature of vorticity is thus eliminated.

Remark on spanwise positioning of nodes

Parametric bicubic patches of the Ferguson type used in this study guarantee second derivative continuity. However, the node spacing has an important effect on the quality of fit. If two neighboring patches have widely varying lengths, the tangent vectors at the common boundary will be too high for the smaller one, causing loops, and resulting in excessive surface areas as well as area related integrals over the patch.

On the other hand, the piecewise linear distribution of vorticity dictates another criterion in the selection of nodal positions. A linear segment should be terminated before the

error in the linear representation is excessive, in order to
maintain the higher order terms at a minimum.

Induced Velocities

It is necessary now to compute the induced velocity due
to the entire vortex sheet, bound and free portions, at a
number of points on the free portion, namely, the patch nodes.
Equation 22 is used. The induced velocities of each panel,
Equation 21 (a generalization of Equation 20), are summed for
all panels representing the vortex sheet. If other singulari-
ties are present, such as solid boundaries represented by
source panels or other lifting surfaces represented by vortex
panels, their induced velocities would be added, too. Source
panels induced velocities are given by an expression similar
to Equation 20, except that the vortex strength is replaced
by source strength, and the $\hat{t}\times$ term is dropped (18).

The surface integral in those equations is not suitable
for closed form evaluation, unfortunately, and a numerical
quadrature is employed (Chapter V).

Symmetry

Computations can be greatly reduced by taking advantage
of the symmetry of the configuration about the y=0 plane.
Letting the physical quantities be expressed for the "left-
hand half" of the wing in terms of those on the "right-hand

half" (primes are used for the left side), then:

$$x' = x$$

$$y' = -y$$

$$z' = z$$

for the vorticity unit vectors:

$$\hat{t}_1 = x_u\hat{i} + y_u\hat{j} + z_u\hat{k}$$

$$\hat{t}_1' = -x_u\hat{i} + y_u\hat{j} - z_u\hat{k} \tag{39}$$

$$\hat{t}_2 = x_v\hat{i} + y_v\hat{j} + z_v\hat{k}$$

$$\hat{t}_2' = -x_v\hat{i} + y_v\hat{j} - z_v\hat{k} \tag{40}$$

for the distance from the elemental vortex to a point in space:

$$\delta x' = \delta x = \xi - x$$

$$\delta y' = \eta + y; \quad \delta y = \eta - y \tag{41}$$

$$\delta z' = \delta z = \xi - z$$

Again, $\vec{\xi}$ is the position vector of the point at which the induced velocity is to be computed, $\vec{x}$ is that of the vortex element, and subscripts u and v denote partial derivatives with respect to these parameters. In Figure 14, these various quantities are depicted.

The displacements in the wake elements are mirror imaged on the left side from those computed on the right side; thus, the panel symmetry relations (38) hold.
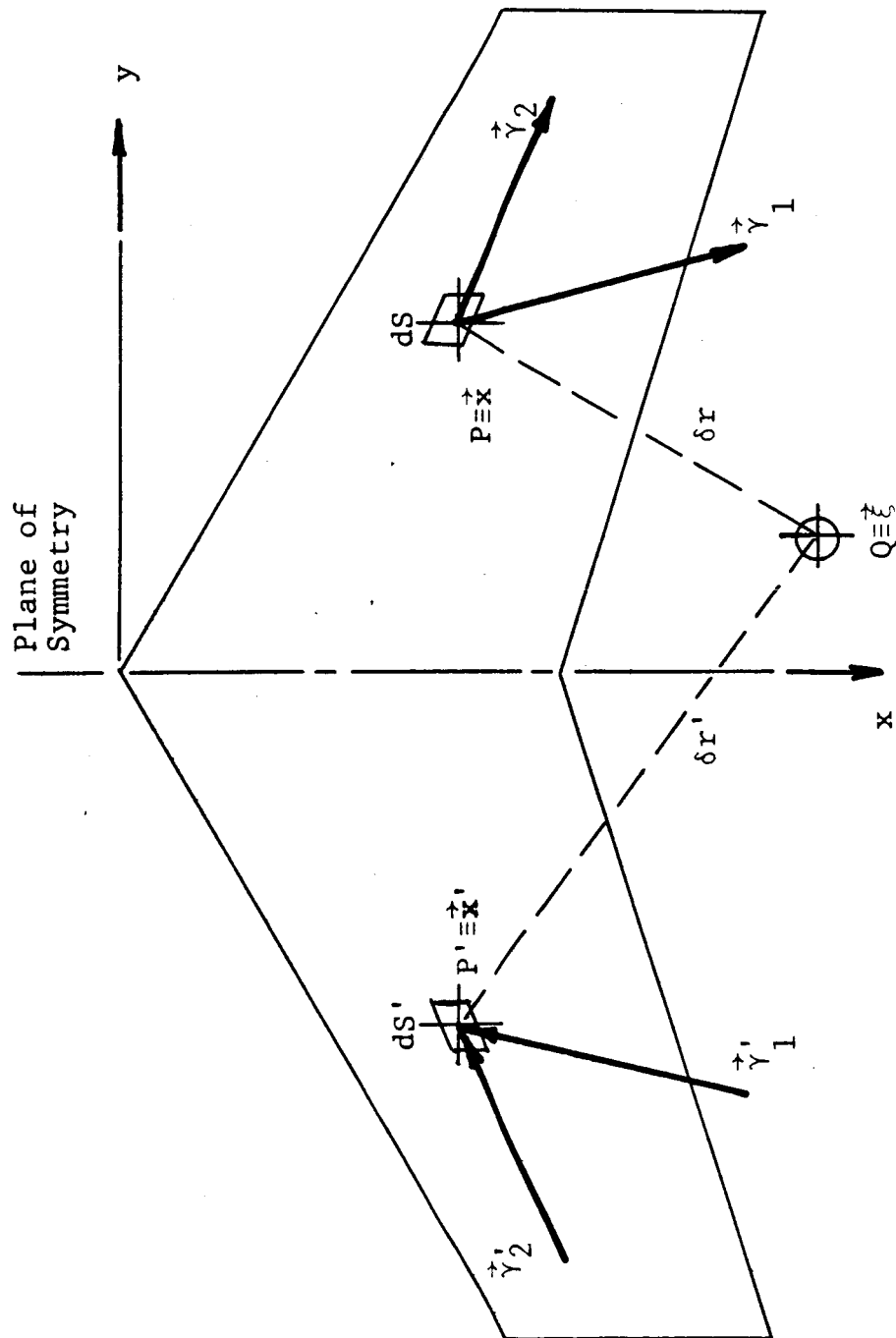
Figure 14. Symmetry of geometric parameters

Procedure to Compute Rollup

Initial conditions and sheet length

The proposed method is an iterative procedure where an initial shape for the free portion of the vortex sheet must be assumed. The most logical one would be to extend the trailing edge in the direction of the free stream velocity, since all sections of the sheet has gone through the trailing edge as they were being shed from the wing. The sheet is extended to a downstream station far enough so that the induced effects at the areas of interest (e.g., the empennage) become negligible. An additional extension is required to promote adequate influence for the rollup of original portion. In the latter portion, accurate rollup is not of essence, rather, its simulation of the fact that the vortex sheet is in reality semi-infinite in length is the intended purpose (Figure 15).

The free portion of the sheet is divided in three regions:

- Region I in which accurate estimates of induced velocities are needed.

- Region II is an extension to such distance beyond which the rollup effects are negligible everywhere in region I.

- Region III is a further extension to such distance beyond which vorticity effects are negligible in region I and II. The various streamwise stations (or spanwise or u=constant curves) are those along which the patch corners or nodes are located, and are numbered from 1 at the trailing edge to m_{III}.

III
Region to simulate
semi-infinite sheet

II
Region where
rollup affects
Region I

I
Region of
concern

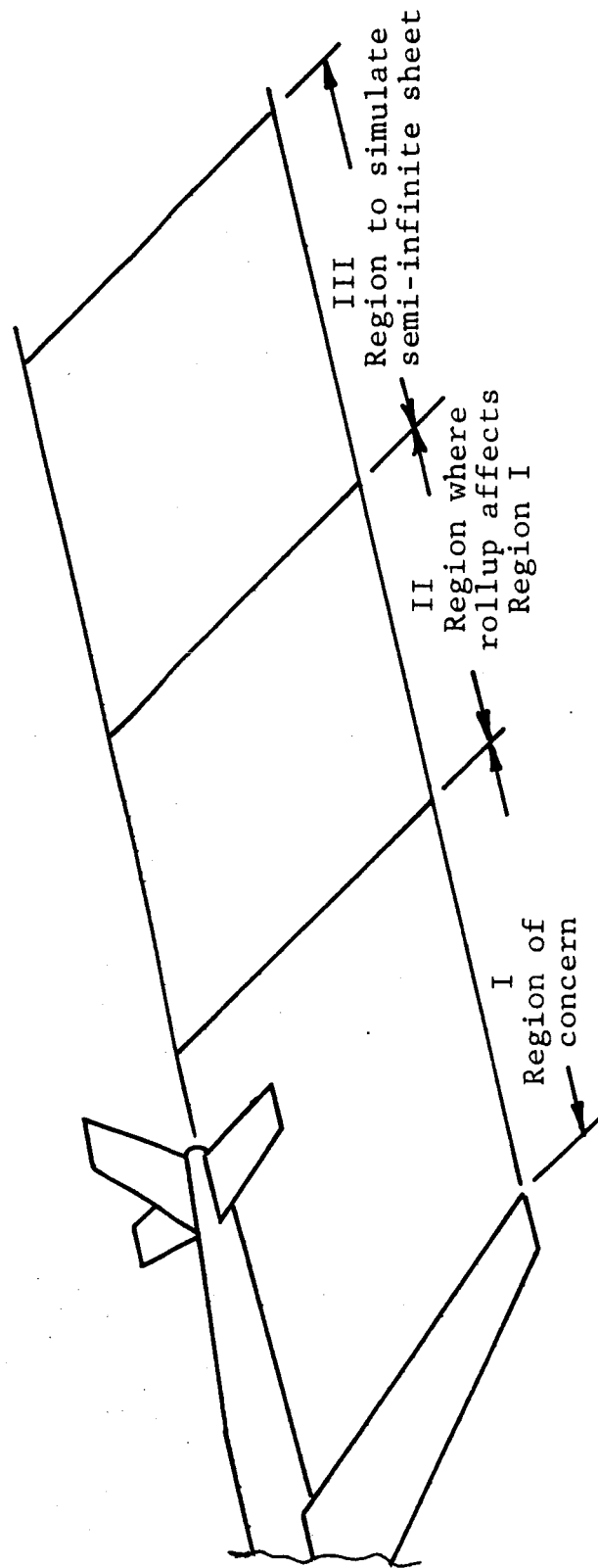Figure 15. Breakdown of trailing vortex sheet for computation purposes

Computation scheme

The following steps are performed to obtain an approxima-
tion of the rolled-up shape of the vortex sheet.

1. The induced effects of the entire initial sheet at
    the nodes of stations 1 and 2 are computed.

2. The induced velocities at station 1 nodes are re-
    quired for computing the downwash and sidewash angles
    at the nodes, such that the resultant velocity

$$\vec{V}_j = (V_\infty + \Delta V_{x_j})\hat{i} + \Delta V_{y_j}\hat{j} + \Delta V_{z_j}\hat{k} \qquad (42)$$

where the V's are the induced velocity components,
coincides with the tangent vector $\vec{x}_{u_j}$. The magnitude
of $\vec{x}_u$ should be approximately equal to the arc length
of a v=constant curve through the particular node on
station 1 between this node and the corresponding
one on station 2. Thus:

$$\vec{x}_{u_j} = \frac{\vec{V}_j}{|\vec{V}_j|} \ell_j \qquad (43)$$

where ℓ is approximated by the chord length $|\vec{x}_{2j}-\vec{x}_{1j}|$
for the node pair in question. The nodal displace-
ments are zero.

3. At the nodes of station 2, displacements at the nodes
    are computed. The time elapsed from shedding to the
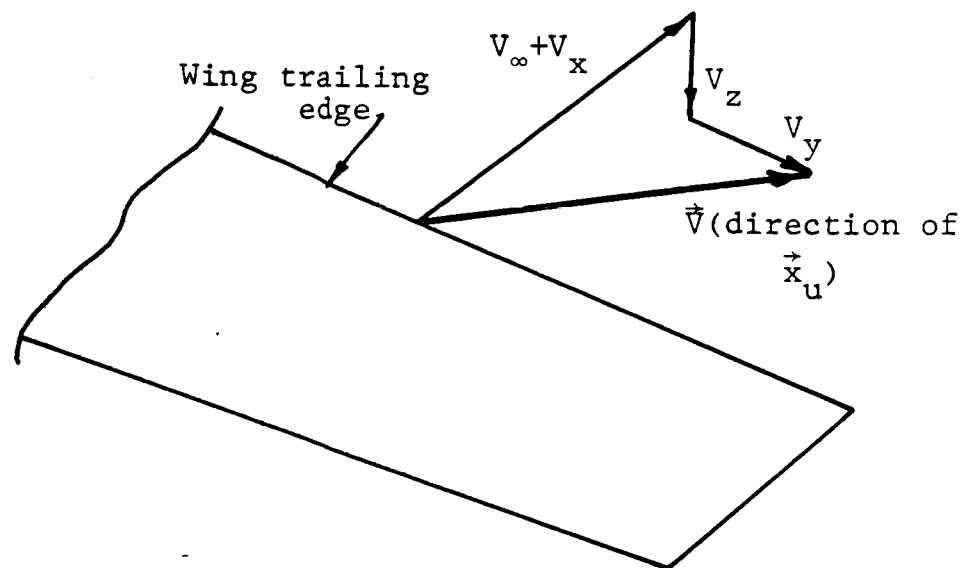   position along station 2 is:

Figure 16. Boundary condition at wing trailing edge

$$t_{2,j} = (x_{2,j} - x_{i,j})/V_\infty \quad j = 1, 2, \ldots, n+1 \quad (44)$$

During this time t, the induced velocities vary from those induced at station 1 to those at station 2. The average velocity is used, so that the displacement for each node at station 2 is:

$$\Delta \vec{x}_{2,j} = \frac{1}{2} t_{2,j} (\vec{V}_{i,j} + \vec{V}_{2,j}) \quad j = 1, 2, \ldots, n+1 \quad (45)$$

Thus, the position vectors are obtained for station 2 nodes:

$$\vec{x}_{2,j}^{1} = \vec{x}_{2,j}^{0} + \Delta \vec{x}_{2,j} \quad (46)$$

The superscript refers to the computation cycle, zero being the initial condition. The treatment of the tangent vectors at the three remaining boundaries is presented later in this chapter.

4. For all the remaining stations, 3 to m_{III}, the incremental nodal position vectors are set equal to those at station 2. The reasoning is that the vortex sheet past station 2 has passed through that curve at some earlier time.

5. The second computation cycle is similar to the first, except that now the third station (i=3) is modified according to the following:

$$\Delta \vec{V}_{i,j}^{2} = \vec{V}_{i,j}^{2} - \vec{V}_{i,j}^{1} \quad j = 1, 2, \ldots, n+1 \quad (47)$$

$\Delta \vec{V}$ is an incremental velocity at station 3 to repre-
sent the acceleration of the particles between sta-
tions 2 and 3. Now, the time elapsed is

$$t_{i,j} = (x_{i,j} - x_{i-1,j})/V_\infty \qquad (48)$$

Then, the incremental displacement $\Delta \vec{x}$ is:

$$\Delta \vec{x}_{i,j} = \frac{1}{2} t_{i,j} (\Delta \vec{V}^2_{i,j} + \Delta \vec{V}^2_{i-1,j}) \qquad (49)$$

6. For stations 4 to m_{III}, the incremental nodal posi-
   tion vectors are equal to those of station 3 nodes,
   and so are the tangent vectors at the tip.

7. The cycle is repeated m_{II} times, (for i values up
   to and including m_{II}), to obtain the relaxed wake
   shape, so that for the kth cycle:

$$\Delta \vec{V}^k_{i,j} = \vec{V}^k_{i,j} - \vec{V}^{k-1}_{i,j}$$

$$t_{i,j} = (x_{i,j} - x_{i-1,j})/V_\infty$$

$$\vec{x}^k = \vec{x}^{k+1} + \frac{1}{2} t_{i,j} (\Delta \vec{V}_{i,j} + \Delta \vec{V}_{i-1,j}) \qquad (50)$$

$$i = 2,3,4,\ldots, k+1$$

Particle motion due to a vortex is not linear. An
assumption of linearity is valid only for small time segments.
In order to relieve this restriction, circular motion about
each elemental vorticity is approximated as follows.

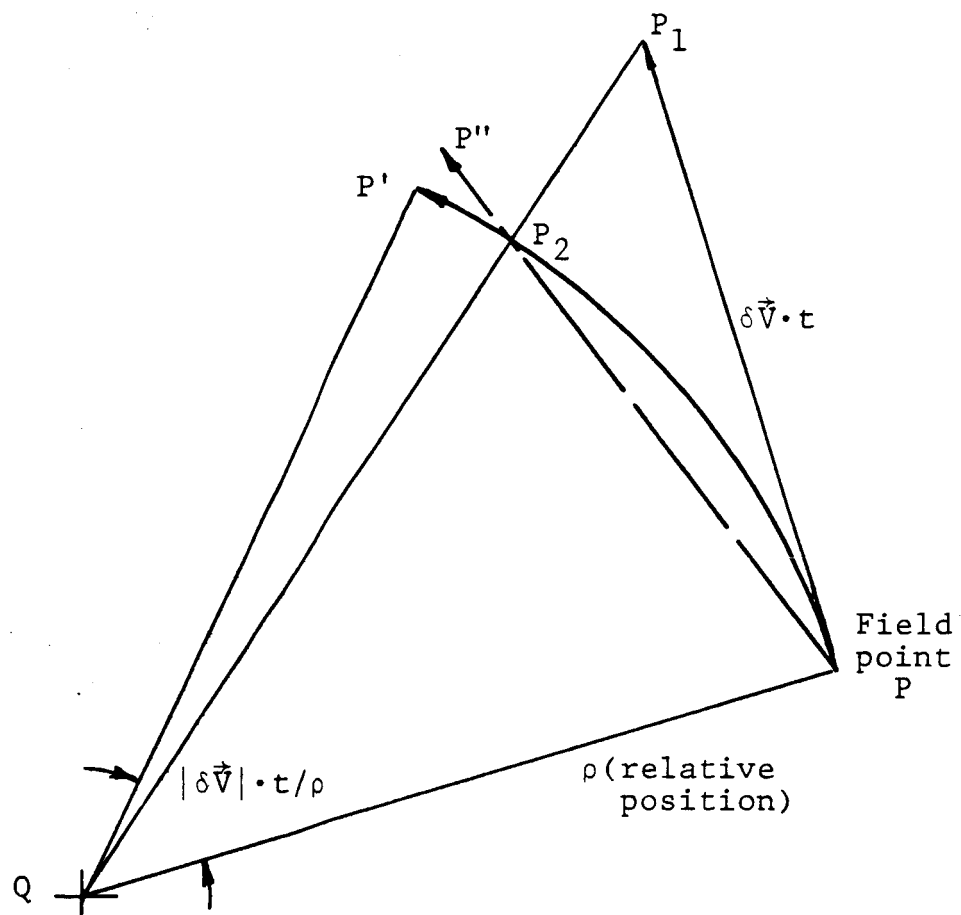In Figure 17, let point P be a field point under the

Figure 17.   Correction for non-linearity of vortex motion

influence of a vortex element at point Q. The distance between them is ρ. The true updated position of P is P', resulting from circular motion about Q. P_1 is the new position using linear motion approximation which can be easily obtained, but is obviously inadequate unless $\rho >> |\delta\vec{V}\cdot t|$. Point P_2 is obtained by multiplying the vector $\vec{P}_1 - \vec{Q}$ by the ratio $\rho/|\vec{P}_1 - \vec{Q}|$. Then, P" is obtained by multiplying the vector $\vec{P}_2 - \vec{P}$ by the ratio $|\delta\vec{V}\cdot t||\vec{P}_2 - \vec{P}|$, so that $\vec{P}" - \vec{P}$ has the same magnitude as the induced effect $\delta\vec{V}\cdot t$. For moderate angles (up to $\pi/2$), P" is a reasonable approximation of P'.

Tangent vectors

The free portion of the vortex sheet is refitted after each displacement. An evaluation of the tangent vectors in transverse direction to the boundary is required. In step 2, the tangents $\vec{x}_u$ were evaluated at the wing trailing edge. The tangents $\vec{x}_u$ at station m_{III} (the last or pseudo infinity station) are assumed parallel to the free stream velocity. Due to symmetry, the tangents $\vec{x}_v$ at the symmetry plane are perpendicular to that plane. The tangent vectors of the remaining boundary, the tip vortex, are discussed next.

Tangent vectors at the tip vortex

First, the direction of the vector is determined as follows: By referring to Figure 18a, consider the current
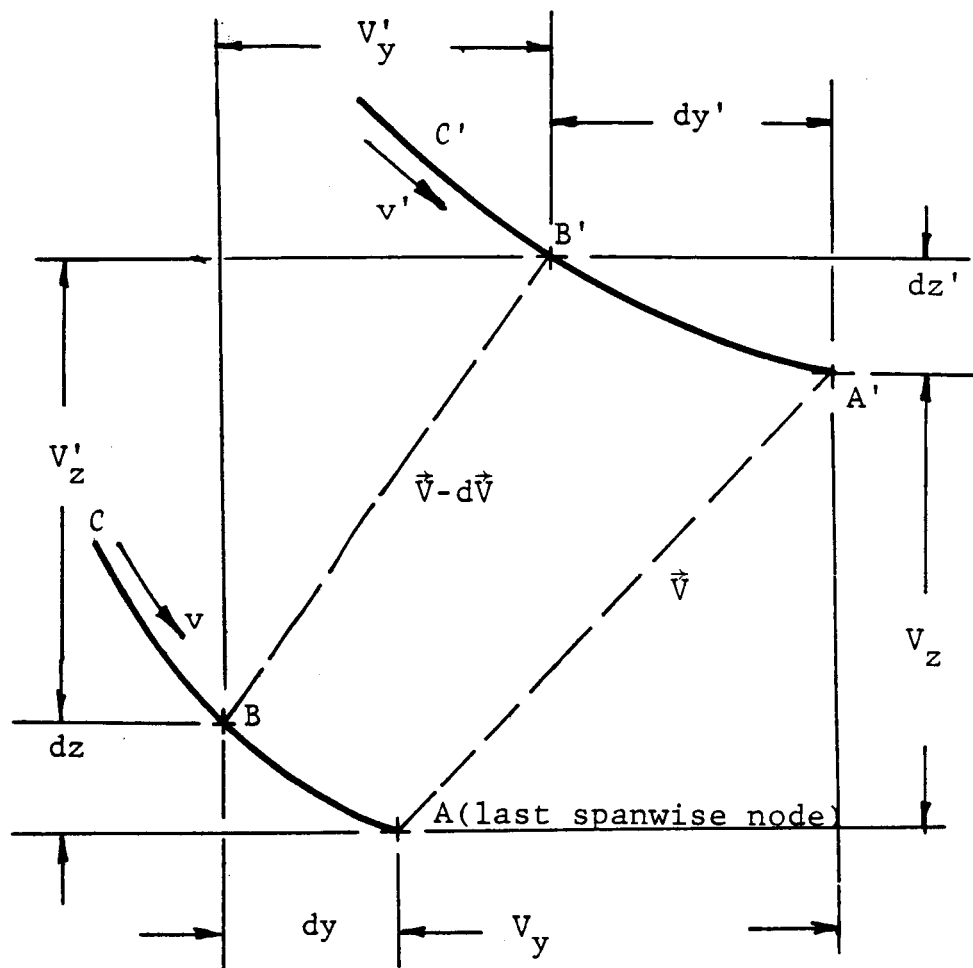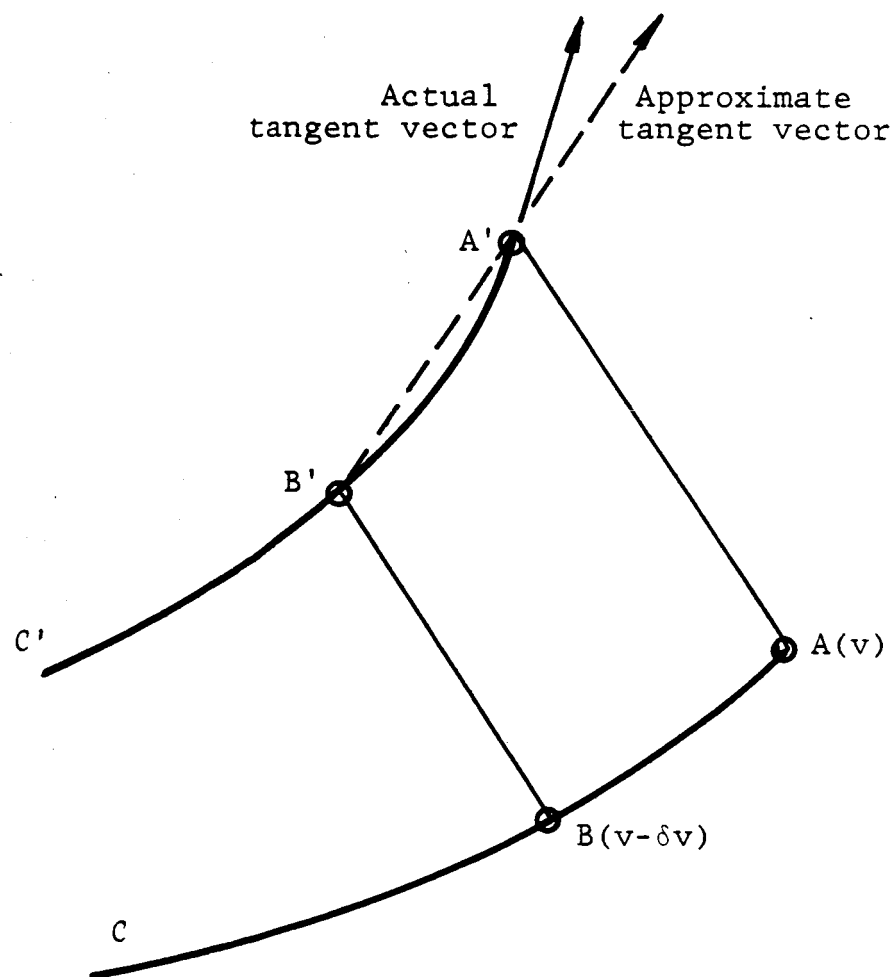
Figure 18a.   Exact tangent vector computation

Figure 18b. Approximate tangent vector computation

section in the sheet represented by curve C. The tip point A has the position vector $\vec{x} \equiv (y, z)$. The y and z coordinates are those of interest since changes in the x-direction are assumed negligible. Point B is a point on curve C just inboard of A whose position vector is $(\vec{x} - d\vec{x}) \equiv (y-dy, z-dz)$. The parameter v assumes the value v and v - dv at points A and B, respectively. Curve C' represents the updated shape of the vortex sheet after the next cycle, that is, after a time t has elapsed since the particles have moved from the upstream station, as in Equation 48. The induced velocity vectors at points A and B are $\vec{V}$ and $\vec{V} - d\vec{V}$, leading to new positions A' and B', with position vectors $\vec{x}'$ and $\vec{x}' - d\vec{x}'$. Thus, the tangent to the curve at A' has the components dy' and dz', where

$$dy' = dy + dV_y t \quad \text{and}$$
$$dz' = dz + dV_z t,$$

or the components y_v' and z_v', the length components of the tangent vector, where

$$y_v' = \nu(y_v + (V_y)_v t \quad \text{and}$$
$$z_v' = \nu(z_v + (V_z)_v t).$$

ν is a scale factor which can be obtained by equating the magnitude $[y_v'^2 + z_v'^2]^{\frac{1}{2}}$ to the arc length of the last segment of the curve, approximated here by its chord length

$[(y_{n+1}' - y_n')^2 + (z_{n+1}' - z_n')^2]^{\frac{1}{2}}$. Therefore,

$$v^2 = \frac{(y'_{n+1} - y'_n)^2 + (z'_{n+1} - z_n)^2}{(y_v + (V_y)_v t^2 + (z_v + (V_z)_v t)^2}$$

Note that

$$(V_y)_v = \frac{\partial V_y}{\partial v} \quad \text{and} \quad (V_z)_v = \frac{\partial V_z}{\partial v}$$

can be obtained by differentiating Equation 22 with respect to v using Leibniz' rule. Since the limits of integration are constant, such differentiation is merely performed on the integrand.

The evaluation of $\vec{V}_v$ would be performed by numerical quadrature in the same fashion as $\vec{V}$ itself, necessitating the near doubling of computations to be performed. Thus, an approximation is adopted as shown in Figure 18b. A point (B) is selected inboard of the tip (A) at a parameter value δv less than that at the tip. δv is chosen small so the chord B'A' represents the tangent vector of the updated curve C' at the tip A'. The position of B' is computed in the same manner as the panel nodes.

CHAPTER V:

DESCRIPTION OF COMPUTER PROGRAM

Introduction

In this chapter, the computer program to perform the computations required for the algorithm described in Chapter 4 is presented. It is written in FORTRAN 77 in a structured, modular form for easy expansion, upgrading, and adaptation to an aerodynamic analysis system.

Major Module Flowchart

A flowchart showing the major functions is shown in Figure 19. Each major function or module is detailed further. Three sets of streamwise panel rows are used:

- The bound vortex panels which are not updated.
- The updatable panels at which the displacements are calculated.
- The slaved panels which are updated to the last station evaluated. (Correspond to those of Region III. See Figure 16.)

The "updatable row" repetition constitutes the relaxation cycle iterations. The entire wake update is repeated for the rows of Regions I and II which the induced velocities, displacements and tangent vectors are re-evaluated. The
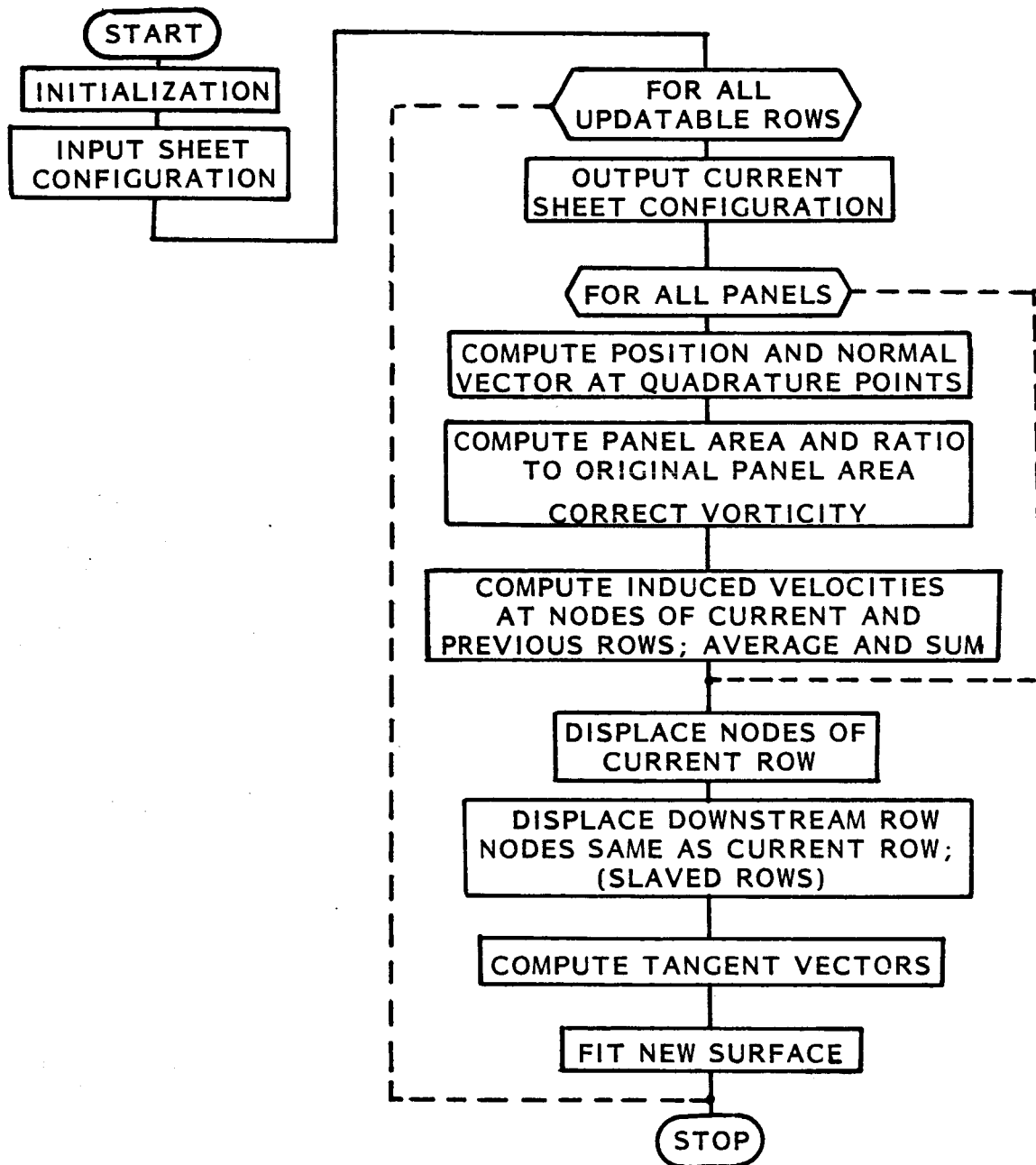
Figure 19. Major function flowchart

results could be output on an external file in the same format as the inputs and the program re-run using those for a better approximation, although this was not done in the present study. As will be shown in Chapter VI, the results obtained from the first iteration were quite satisfactory. In the following, the various details are discussed.

Surface fit

This module merely fits parametric cubic curves in the u and v directions independently, resulting in the tangent vectors at the nodes in both these directions. The twist vectors are not obtained, for simplicity, and due to their minimal effect on the quality of fit. However, if necessary, they should be computed here. The Thomas' algorithm is used to solve the set of tridiagonal equations as explained in Chapter II.

Quadrature points

This module interpolates the wake surface within a patch for a set of 25 points, (see Table below), used for quadrature, to obtain the position and tangent vectors, $\vec{x}$, $\vec{x}_u$ and $\vec{x}_v$. Then, the latter two are used to obtain the normal vectors $\vec{x}_u \times \vec{x}_v$ and their magnitudes, and store these data for use by other portions of the program within the patch loop. This module uses another one to obtain the poly-nomial coefficients of the patch, given the nodal positions and tangents. The latter are merely the partial derivatives

of the position polynomials, with respect to the parameters
u and v. These data are used in obtaining the deformed or
stretched patch area in order to compensate for the stretch-
ing, as well as for evaluating the induced velocity integrals.

Numerical integration

The Gaussian quadrature is used. The integrand is
evaluated at twenty-five points in the interior of each panel
forming a grid of five points in u-direction along five con-
stant v curves. The values of u and v are shown in the table
below. The elemental area is approximated by a weighting
factor for the integrands $a_i a_j$, the values of a_i corresponding
to the grid point is also shown in the Table. The integral

$$\int_0^1 \int_0^1 f(u,v) \, du \, dv$$

is approximated by the double summation

$$\sum_{j=1}^{5} \sum_{i=1}^{5} f(u_i, v_j) \, a_i a_j$$

Gaussian Quadrature Parameters

i	u_i or v_i	a_i
1	0.046910077	0.11846344
2	0.230765345	0.23931434
3	0.5	0.28444444
4	0.769234655	0.23931434
5	0.953089923	0.11846344

Induced velocities

For each of the quadrature points, the values of the
vorticity are interpolated, and the relative position vector
(to the node at which the velocity is being calculated) evalu-
ated for one half of the symmetrical vortex sheet, as well as
the other opposite half. The induced velocity vector induced
by the current patch at the entire set of nodes is obtained
by use of the Gaussian quadrature. These are stored and incre-
mented for all patches of the network. This is done so that
the patch quadrature points are evaluated only once per relaxa-
tion cycle, to reduce the amount of computations. In this
fashion, the bulk of the computations is done in the induced
velocity quadrature.

Typical run statistics

One test case used 15 × 7 panels. The 15 streamwise
rows comprise 3 bound, 7 slaved, and 5 updatable sets. The
run required 105 CPU seconds on the Iowa State University
NAS-AS/6 computer, constituting most of the thirteen dollar
charge. Should this method be used in conjunction with a
potential flow paneling program, two iterations are to be
sufficient, add a small percentage to the total cost.

CHAPTER VI:

RESULTS AND DISCUSSION

The results of the computational method of the present

study are presented in two parts:

1. A wing planform tested for vortex sheet shape

   visualization is modeled numerically and compared

   with the test results to demonstrate the validity

   of the method.

2. The span loading of the wing is altered arbitrarily

   to simulate deployed flaps (or stalled outboard

   panel) is modeled and the results presented to

   demonstrate the ability of the system to handle

   complex loadings.

The first part uses the results of a wind tunnel test con-

ducted in the Boeing Co. Research Wind Tunnel, which is

described next.

The Test Wing

Description of the test

The planform of the wing is shown in Figure 20, along

with the spanwise load distribution, measured experimentally

using pressure taps at various stations. The load distribu-

tion used in the numerical model must be a piecewise linear

distribution of bound vorticity. This modeling is described in the following section.

The flow visualization technique used for this experiment consisted of injecting steam and liquid nitrogen in the airstream at a location upstream of the wing tip. The nitrogen flow rate is adjusted to bring the air and water vapor mixture close to the dew point, so that a small drop in temperature will cause condensation of the vapor and result in a mechanical mixture of air and water droplets. This effect will take place if an adiabatic pressure drop occurs, specifically along the vortex sheet, where the induced velocities are locally high. If the wind tunnel is of the open type and the atmospheric relative humidity is high, and the air temperature is very low, liquid nitrogen would be unnecessary.

Light is applied to a section of the stream past the wing trailing edge through a narrow slit so that only the water droplets at the particular section are illuminated and can be photographed.

A complete description of this and other methods used for this program can be found in references (21, 29). The only available photograph from the test was taken at a section 1.25 spans behind the wing's trailing edge, and is shown in (29), along with computational results discussed later. The flow visualization is illustrated in this report as the dashed line in Figure 22f.
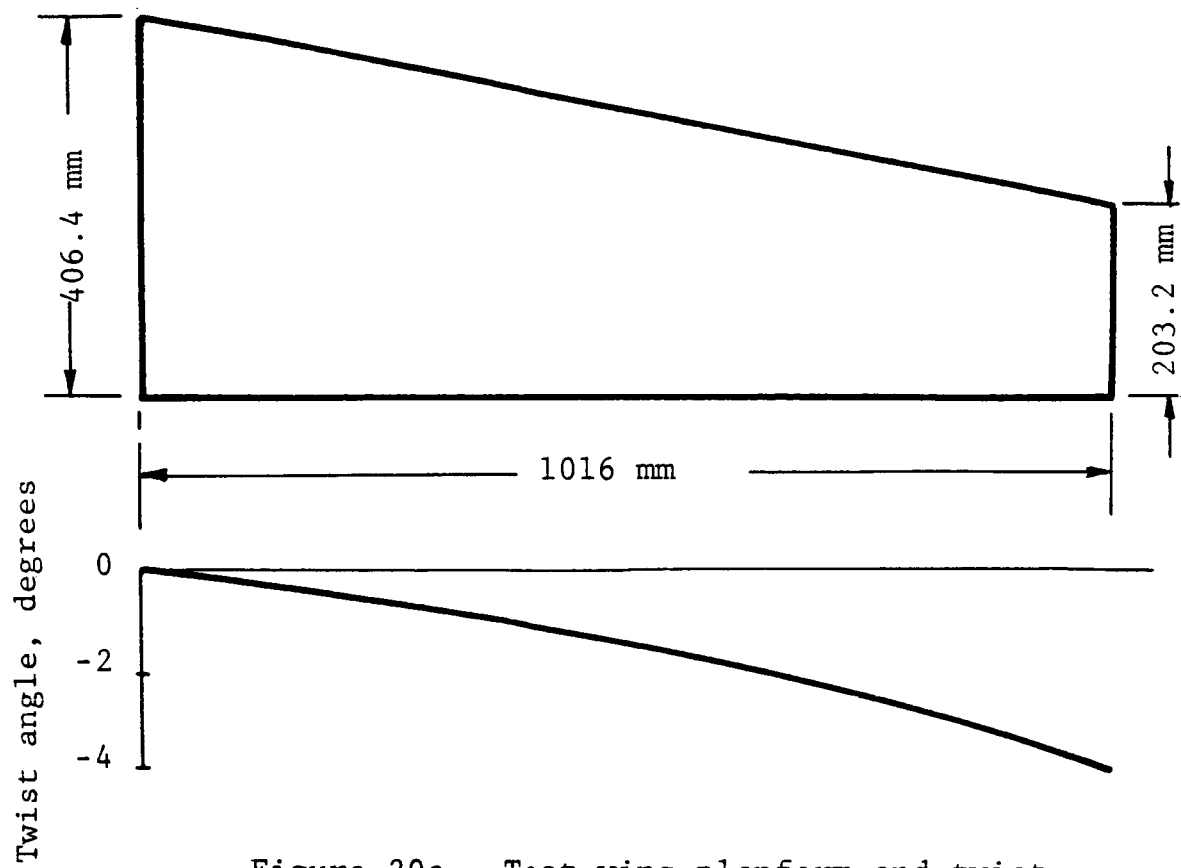
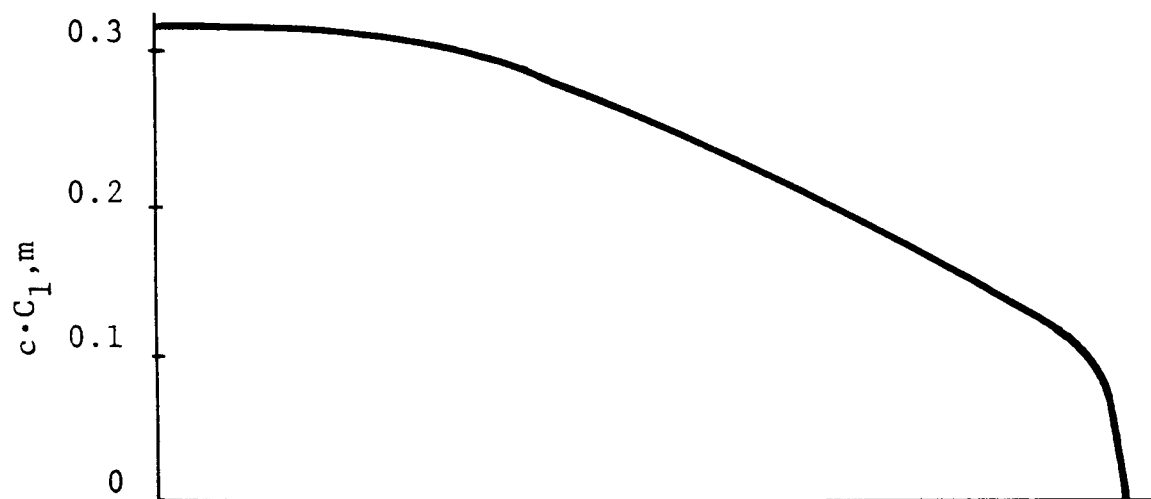Figure 20a.   Test wing planform and twist

Figure 20b.   Test wing span loading (experimental)

Numerical modeling of wing loading

The necessary inputs to the computer program are piece-wise linear vorticities for each panel of the vortex sheet. In this section, the bound (or fixed) portion thereof is discussed.

Since no chordwise loading was published in (29), a distribution similar to aft loaded airfoils was assumed. Three chordwise panels are used. The leading edge is 20% of the chord and a vorticity distribution varying linearly from zero to a maximum value γ_2' depending on the local spanwise load. The middle panel is 40% of the chord with constant vorticity γ_2'. The trailing edge panel is 40% of the chord and returns the vorticity to zero linearly. For a given value of local loading ($c \cdot C_\ell$), the bound circulation Γ can be obtained from:

$$\Gamma = \frac{1}{2} V \, c \cdot C_\ell$$

where: V is the free stream velocity = 26.84ms^{-1} (as in the test)

c is the local chord, meters

C_ℓ is the local lift coefficient.

Γ is also equal to

$$\frac{1}{2}[(\gamma_2+\gamma_1)(x_2-x_1) + (\gamma_3+\gamma_2)(x_3-x_2) + (\gamma_4+\gamma_3)(x_4-x_3)]$$

where: γ_i is the value of γ_2 at the ith chordwise node

x_i is the x coordinate of the ith chordwise node.

Now, $\gamma_1 = \gamma_4 = 0$, $\gamma_2 = \gamma_3 = \gamma_2'$; $x_4 = 0$ since the trailing edge is placed on the y-axis, and x_1, x_2 and x_3 are respectively 1, 0.8, and 0.4 multiples of the local chord. Thus:

$$\gamma_2' = \frac{\Gamma}{0.7c} \; ms^{-1}$$

Due to the linearization of $c \cdot C_\ell$, large variations were found in the values of the shed vorticity when computed using differences. A good approximation was obtained by graphically estimating the slope of the $c \cdot C_\ell$ curve at the various spanwise nodes. These nodes were chosen at $y = 0$, 0.42, 0.67, 0.82, 0.91, 0.96, 0.996, and 1.016 m, according to the considerations discussed in Chapter 4.

The values of the shed vorticity γ_1 are obtained at these stations from:

$$\gamma_1 = \frac{V}{2} \frac{d}{dy} (c \cdot C_\ell)$$

The amount of shed vorticity across panel i is

$$\Delta\Gamma = (\gamma_1|_i + \gamma_1|_{i+1}) \cdot \frac{\Delta y_i}{2}$$

which is equal in a reduction in bound vorticity Γ. Thus, γ_1 and γ_2 at each node are computed and shown in Figure 21. The bound vorticity is represented by the γ_2' values. The shed vorticity near the tip was initially calculated to satisfy Helmholtz' law (see Figure 13), and is shown by point A and the dashed portion of the curve. The value was

32.2. Point B and the solid curve reflect a value of 45. The difference will be discussed later.

Results and discussion of the validated case

The results of the numerical modeling of the test wing described above are presented here. Figures 22a through 22f show sections of vortex sheet at various streamwise stations: 0.35, 0.65, 0.95, 1.25, 1.55, and 2.50. The stations calculated are 0.35, 0.65, 0.95, 1.25, 1.55, 1.88, 2.25, 2.66, 3.1, 3.7, 4.5 and 5.5. The last three stations are in Region III, that is, their shape is identical to the one at 3.1m. The plot at station 2.50 (in Figure 22f) is interpolated between 2.25 and 2.66, and is used to compare with the available experimental results.

First station in the sheet

The trailing edge of the wing is at x=0, and this is where the first station should be. However, the linear distribution of the bound vorticity led to unrealistically large localized vorticity at the trailing edge, especially near the tip, and it was necessary to displace the first station of sheet an arbitrary 0.05 m downstream. The downwash angles thus calculated are more consistent with experience (Figure 23).

Tip vorticity

The computed value of tip vorticity (point A in Figure 21) is inaccurate due to the linear approximations at the tip. The vorticity there is theoreti-
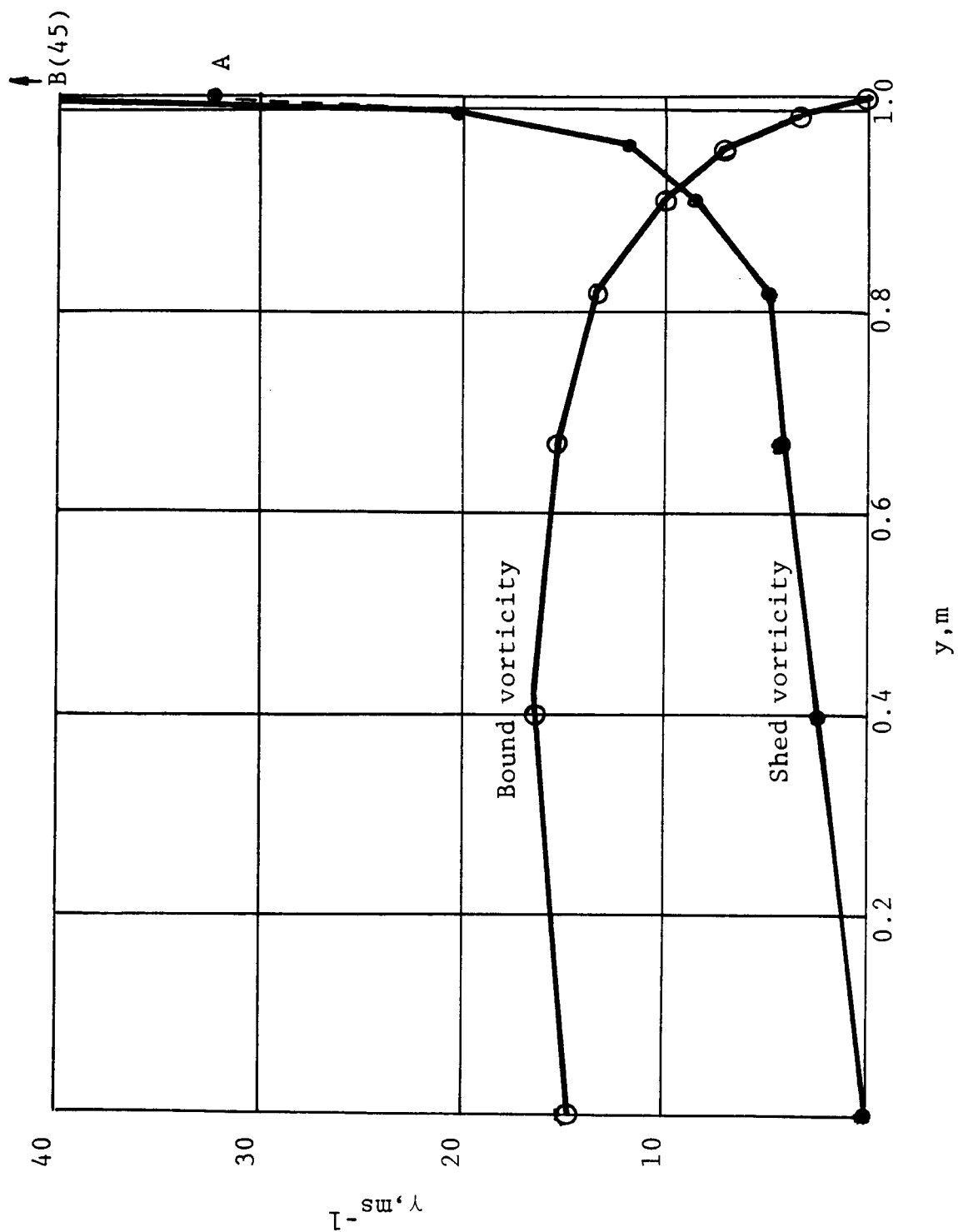
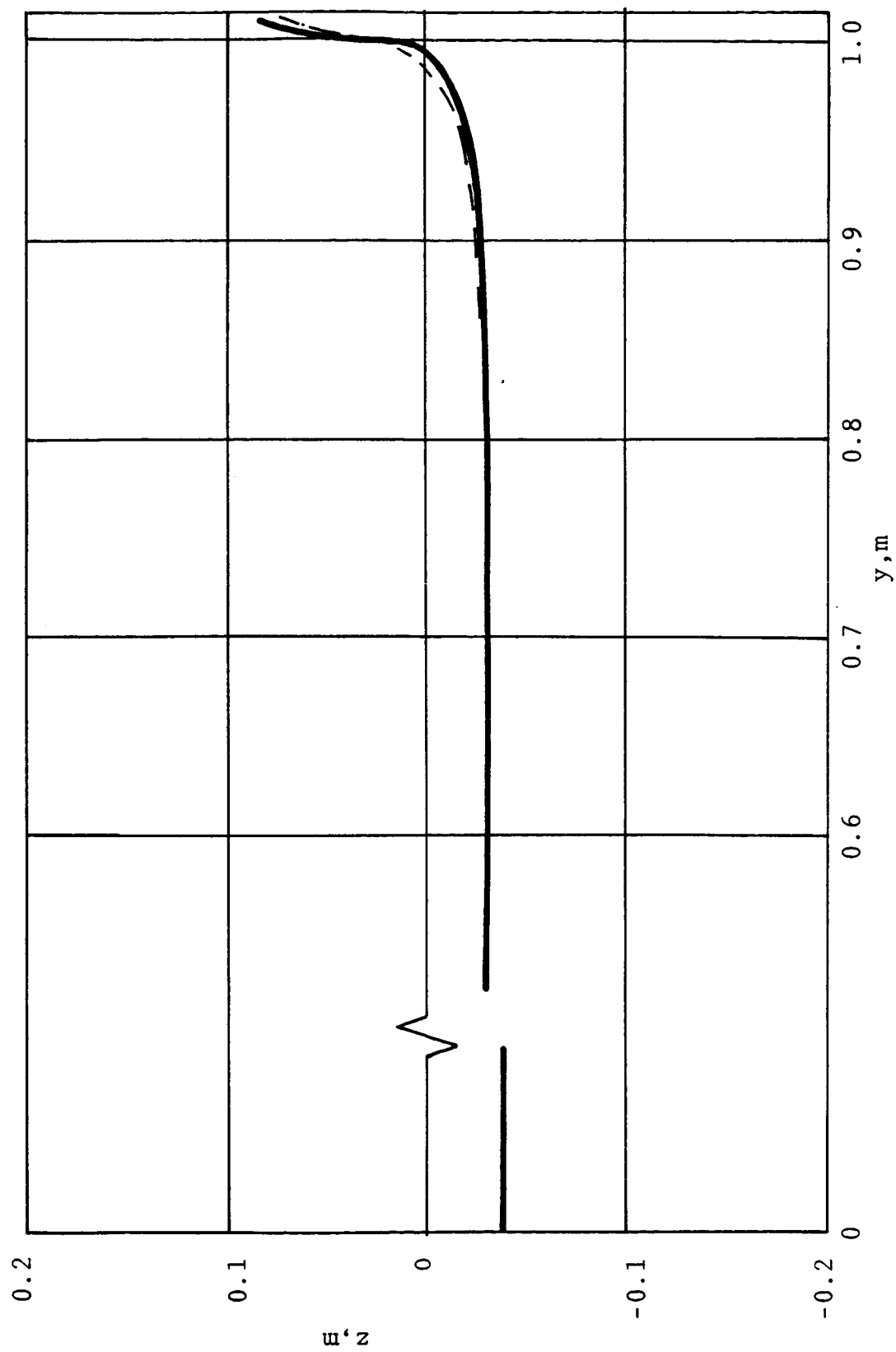Figure 21. Piecewise linear representation of Test Wing vorticity

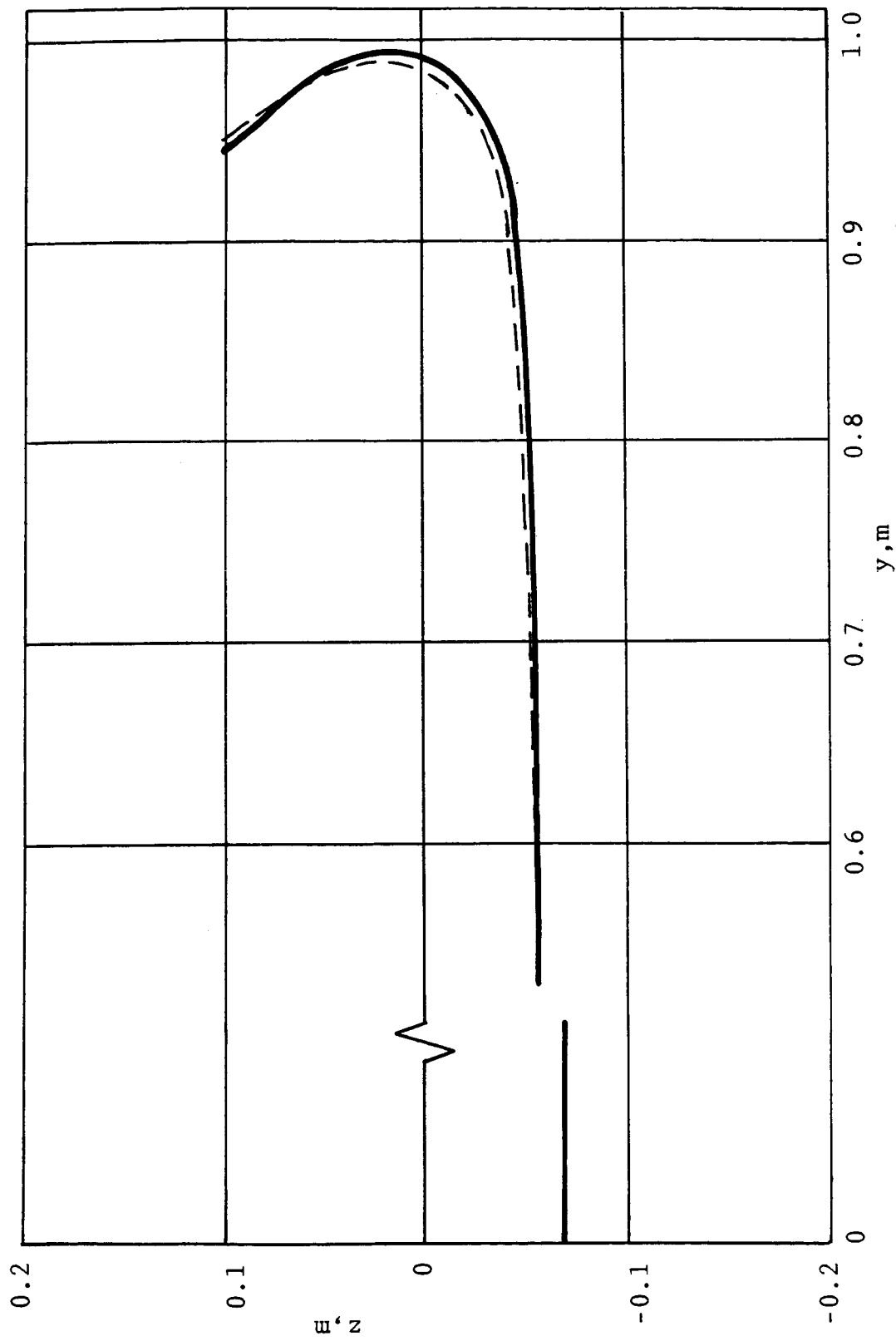Figure 22 a.   Section of vortex sheet at station 0.35

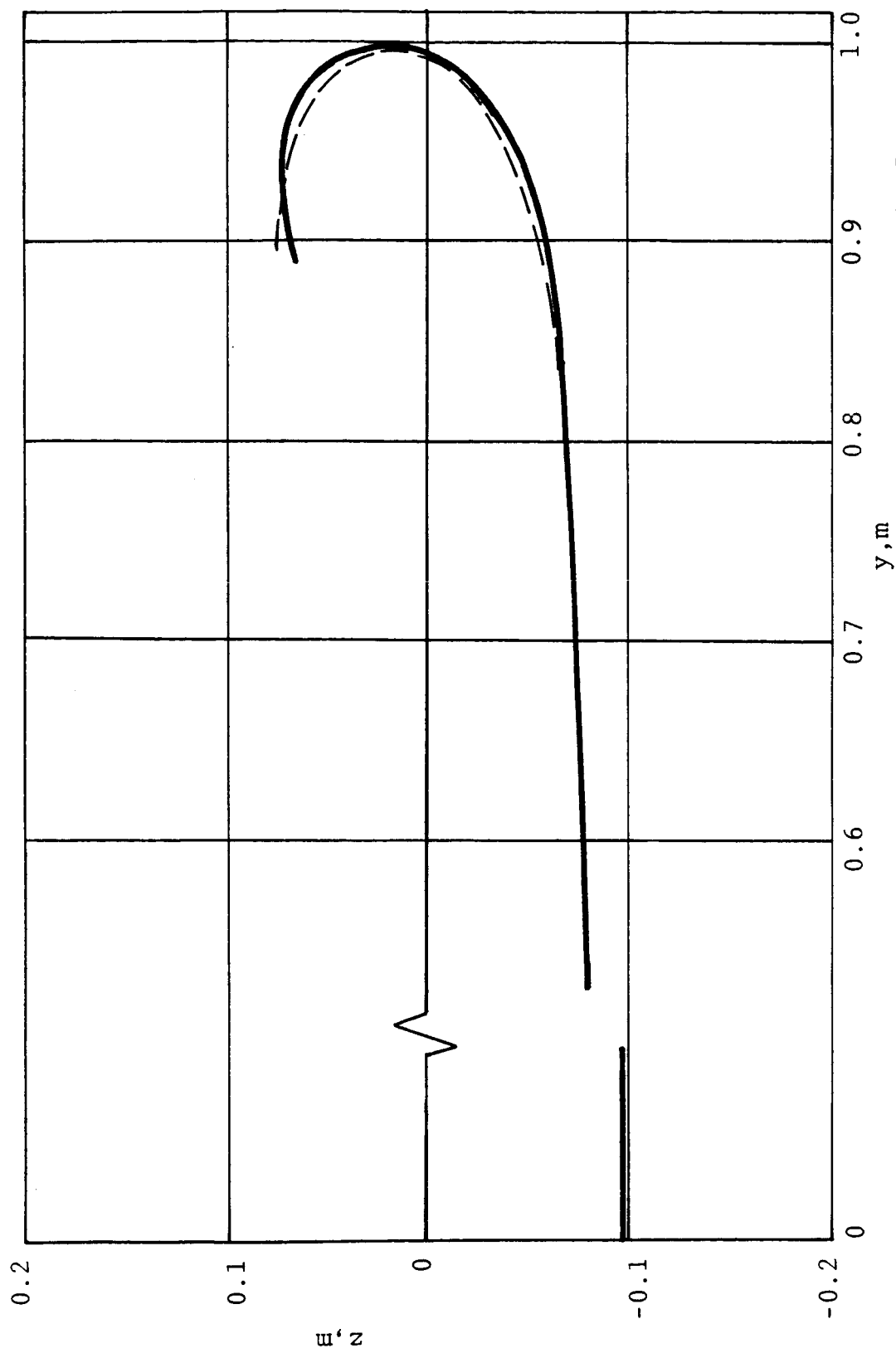Figure 22b. Section of vortex sheet at station 0.65

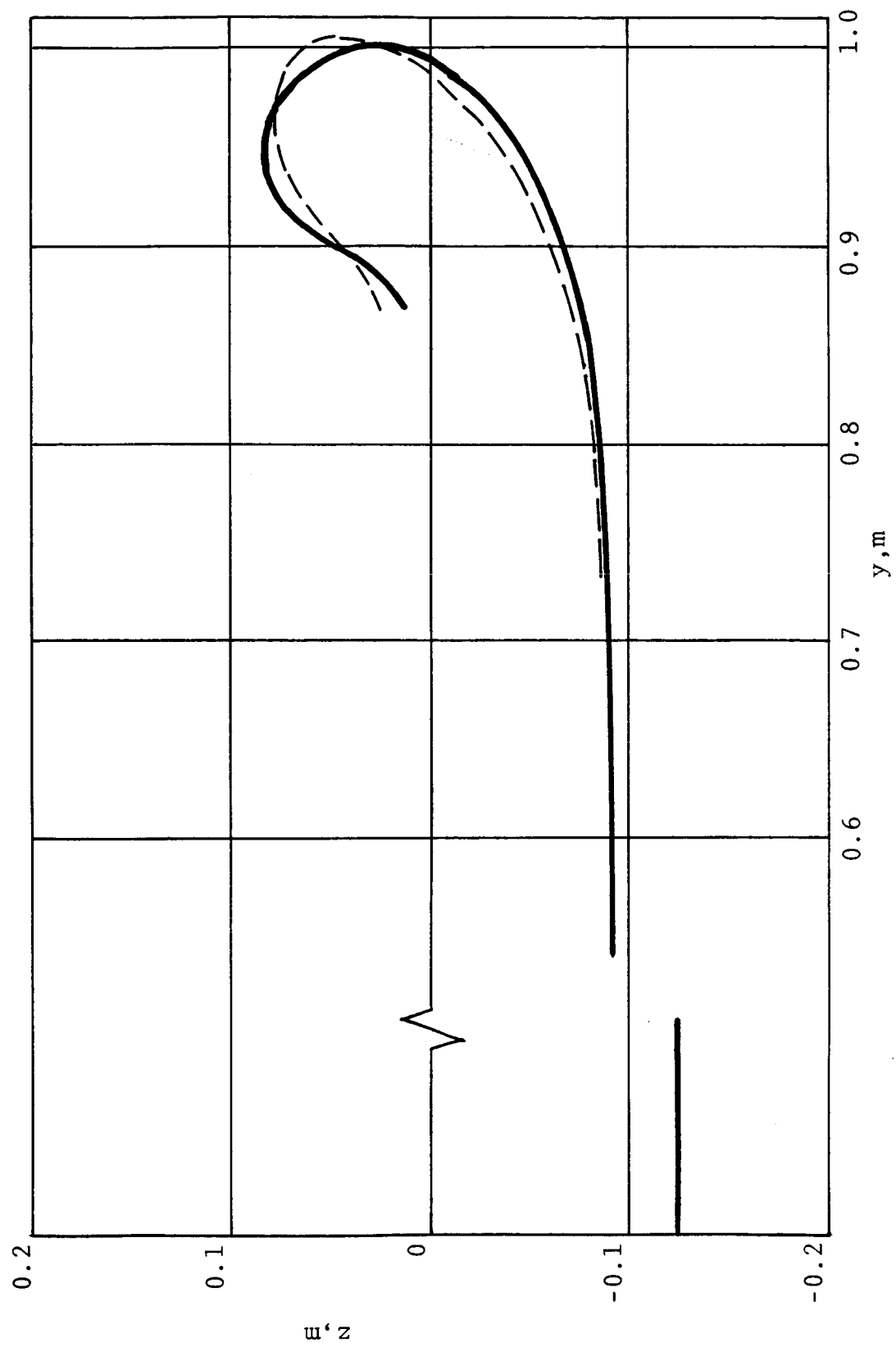Figure 22c. Section of vortex sheet at station 0.95

Figure 22d. Section of vortex sheet at station 1.25
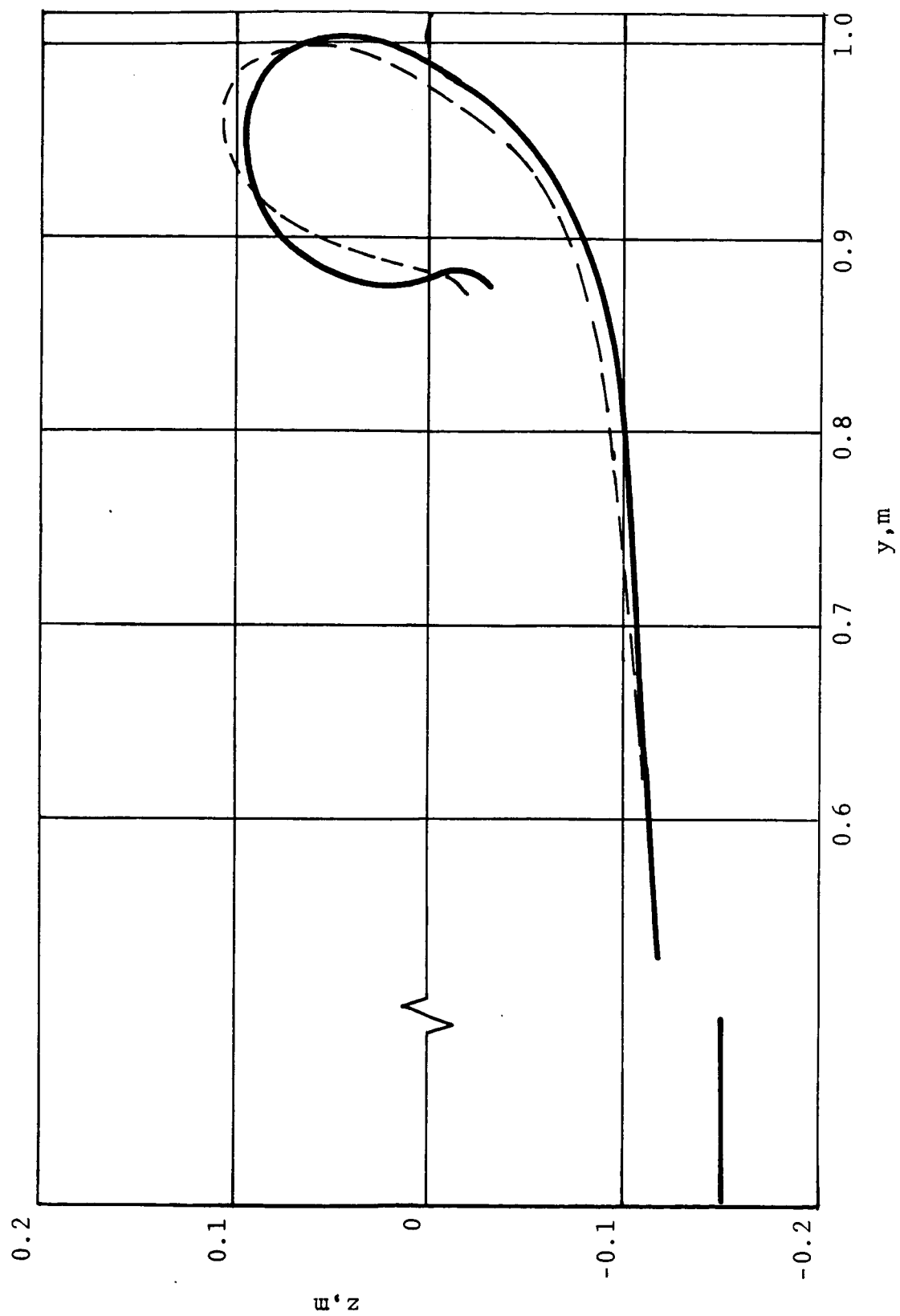
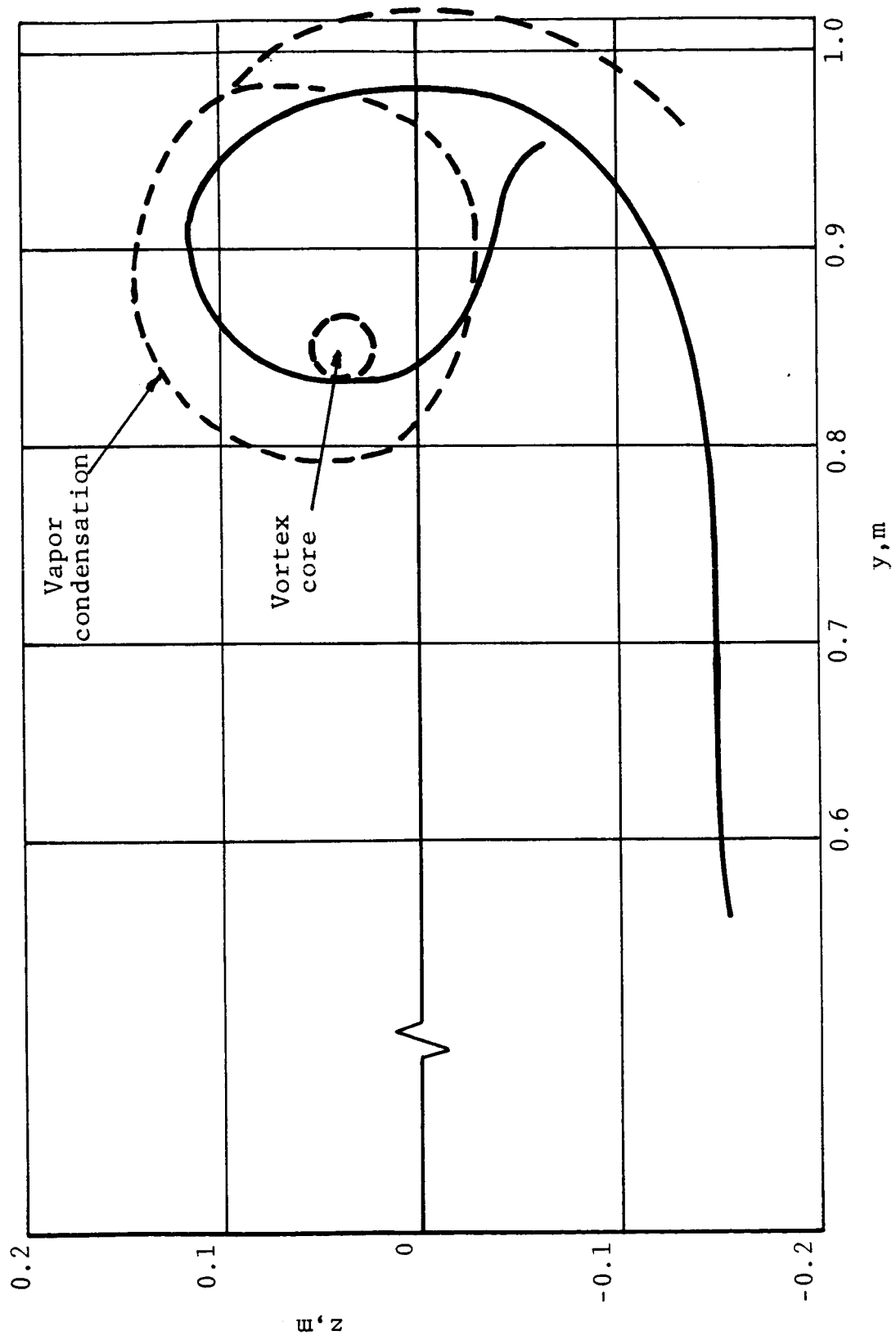Figure 22e. Section of vortex sheet at station 1.55

Figure 22f. Section of vortex sheet at station 2.50 and comparison with test

cally infinite. The results using the calculated value (A) are plotted using the dashed lines. The computed slope at the tip results in a reversal of curvature there, due to the reduced vorticity value and other effects discussed below. The tip vorticity was subsequently increased to 45 (point B) arbitrarily, and improved results were obtained at some of the stations. However, the shapes thus obtained show a fuller curvature and a better "spiral" shape, consistent with intuitive expectations of the true shape.

Two alternatives were considered. The first one was to reduce the spanwise size of a few panels near the tip to improve the vorticity modeling. The result was an excessive proximity of the quadrature points (lumped singularities) and the panel nodes, resulting in numerical problems. Usage of double precision to reduce round off error would have helped only slightly, but would result in doubling the computational resource requirements. Ideally, a closed form integral, albeit approximate, would probably solve this problem. The second was to increase this arbitrary tip vorticity to larger values, e.g., 100, violating Helmholtz' first law, and still resulting in numerical problems similar to those above, now due to the large value of vorticity.

Slope at the tip   The quality of the solution was found to be extremely sensitive to this variable. Originally, it was planned to use the chord of the tip panel to approxi-
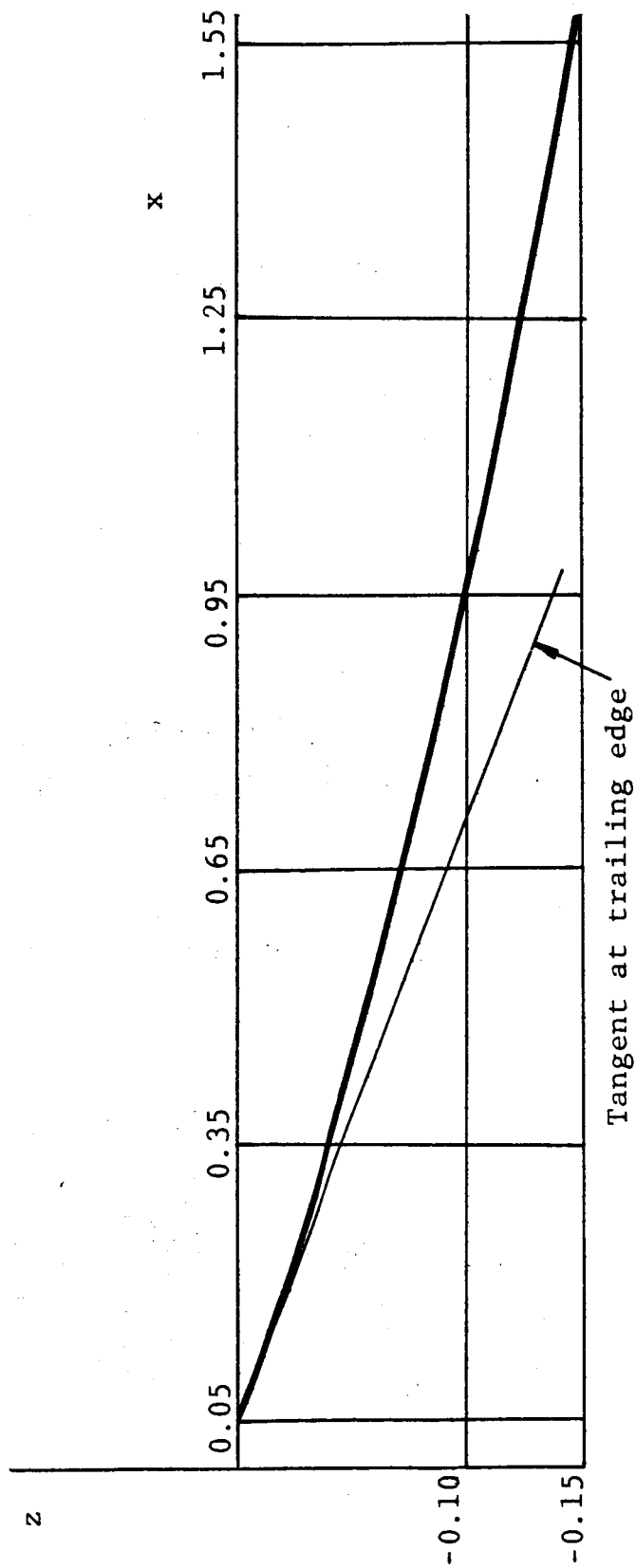
Figure 23. Illustration of downwash variation downstream of wing
at the plane of symmetry

mate the tangent at the last node, and in fact, this was used in the preliminary testing of the method. However, flattening and inflections in the curve near the tip resulted, as expected. The second attempt was to use the bisector of the angle between the chords of the two adjacent panels at the tip, and estimate the magnitude using a heuristic formula. While this was successful in some cases, it failed in most, simply because it is difficult to program logic to account for all possibilities of angle combinations, orientations and relative node positions. In addition, this method is unrelated to the physical aspects of the problem. The method described in Chapter 4 was finally resorted to. The approximation used is essentially an improvement of the tip chord approach. A point is chosen within the tip panel to produce, along with the tip node in a short chord to approximate the required tangent. While some numerical problems are overcome (namely, eliminating the need for a very small tip panel), others resulted. The computed induced velocity at that point is dependent on its position relative to the quadrature points. Thus, its location was varied until the least amount of inflections in the curves were obtained. It seems that the induced velocity there is still somewhat excessive. It also seems that the exact value of the slope (also described in Chapter 4) should be used for better results, that is, to reduce the inflections or eliminate them.

<u>Comparison with test</u>   This is done in Figure 22f. The dashed line labelled "Vapor condensation" is at the center of the bands of illuminated water particles as they appear in the photograph in reference (29), Figure 5.4. The circular area labelled "Vortex core" appears as a dark circle in the photograph. This is the innermost part of the rolled-up sheet, where viscous effects are most prominent. The computed contour is shown with the solid line. The computation was done starting with a flat sheet, and while iterations could have been performed to "relax" the shape to one where the pressure differential across the sheet vanishes, the closeness of the computed and experimental results suggested this was unnecessary for the purpose of this study, which is to test the ability of this modeling to produce realistic predictions of the vortex sheet. In their paper, Butter and Hancock (6) show the results of their relaxation scheme. There, the second cycle's results are close to those of the initial cycle, except in the two stations immediately behind the wing, where the rolled up sheet effects are not included for the first, and only slightly included for the second. It must be noted that the only available photograph of the flow visualization is for a station far enough downstream, that viscous effects have had a considerable effect on the shaping of the sheet. Furthermore, it appears that, if the tip condition were modeled more accurately, a

better approximation would have resulted.

Another consideration is that the test wing has a trapezoidal planform with considerable tip flow, not accounted for in the mathematical model.

Comparison with other computational methods   Reference (29) shows predictions of the sheet shape at the same station, using a very large number of discrete vortex filaments, both inviscid and viscous, the results show the spiral shape is contained between 96% and 101% of the half span. In other words, the roll-up form is too tight, compared with experiment. The calculations of these methods are based on the Trefftz plane scheme (two-dimensional). The results of the current methods are much more realistic.

The Wing with Deployed Flaps

In order to assess the behavior of the present method in predicting vortex sheet rollup resulting from complex wing loading, such as for deployed partial span flaps and partially stalled wings, the loading of the test wing was altered by increasing the lift in the inboard half, as shown in Figure 24, by the bound vorticity curve. A slight dip in lift was included just outboard of the flaps to render the loading more realistic. The remainder is unchanged.

Numerical modeling

The procedure is identical to the one just explained, with the exception of the selection of the number of spanwise nodes. They must be increased where the rates of change in vorticity is high, not only to model it accurately, but to improve the surface fit, as will become evident in the discussion. Twelve spanwise patches were used here, as shown in Figure 24.

Results and discussion

The results are shown in Figures 25a through 25e, for sections of the sheet at stations 0.35, 0.65, 0.95, 1.25, and 1.88. All but the last are very realistic, even though no experimental results are available for comparison. The solution is consistent up to 1.25 half spans downstream. At 1.88 m, the vortex sheet crosses itself. This is interpreted as follows: The nodal displacements are calculated properly for that station, however, the surface fit is done according to a criterion which is not necessarily consistent with the physics of the problem. Second derivative continuity is required in the fit, and this poses constraints on the polynomial degrees of freedom. Thus, the resulting solid curve in Figure 25e is merely a C^2 interpolant of the node points shown. From a physical standpoint, however, a more realistic constraint to impose is the slope of the tangents at the nodes, with values computed from the induced velocity gradient
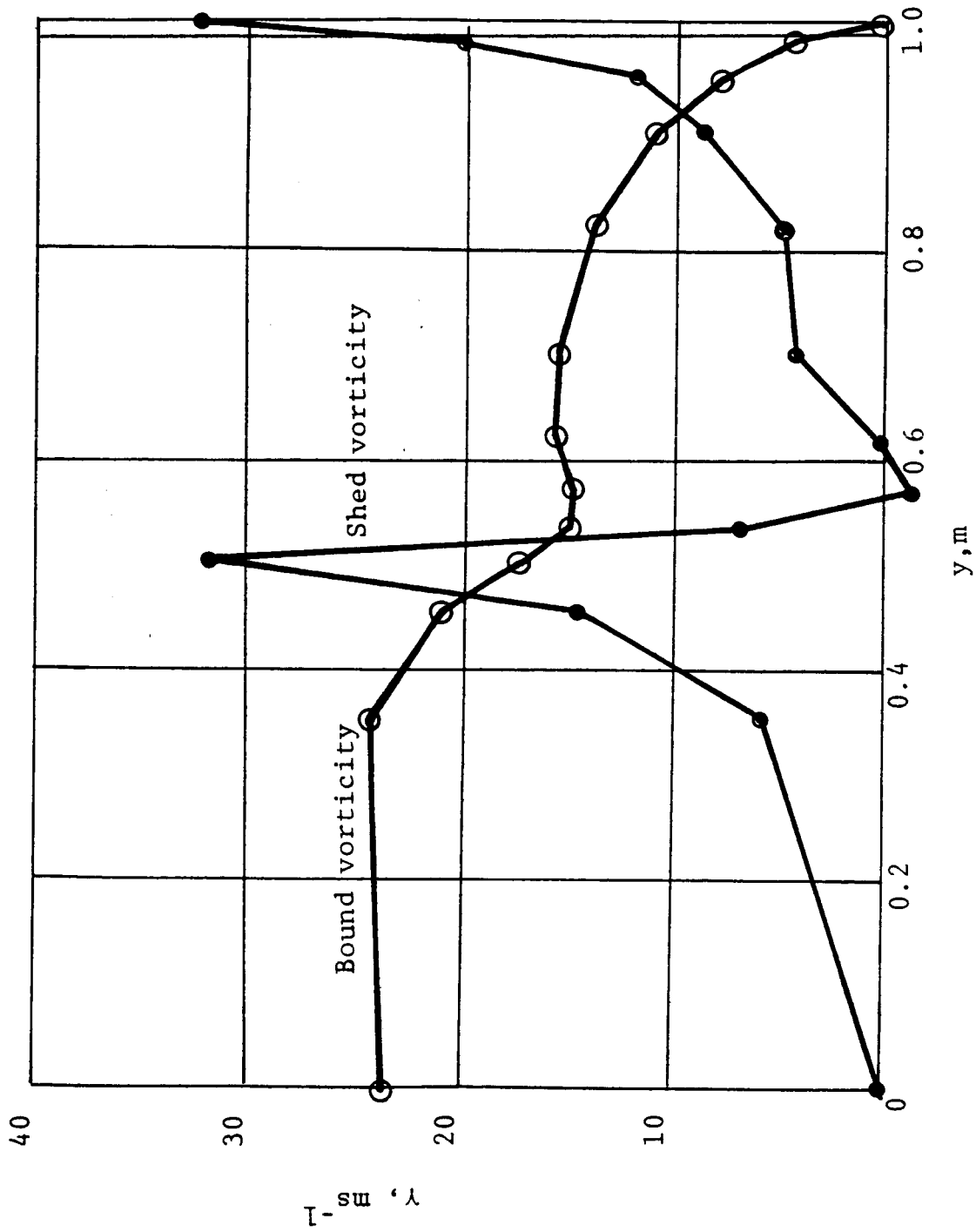
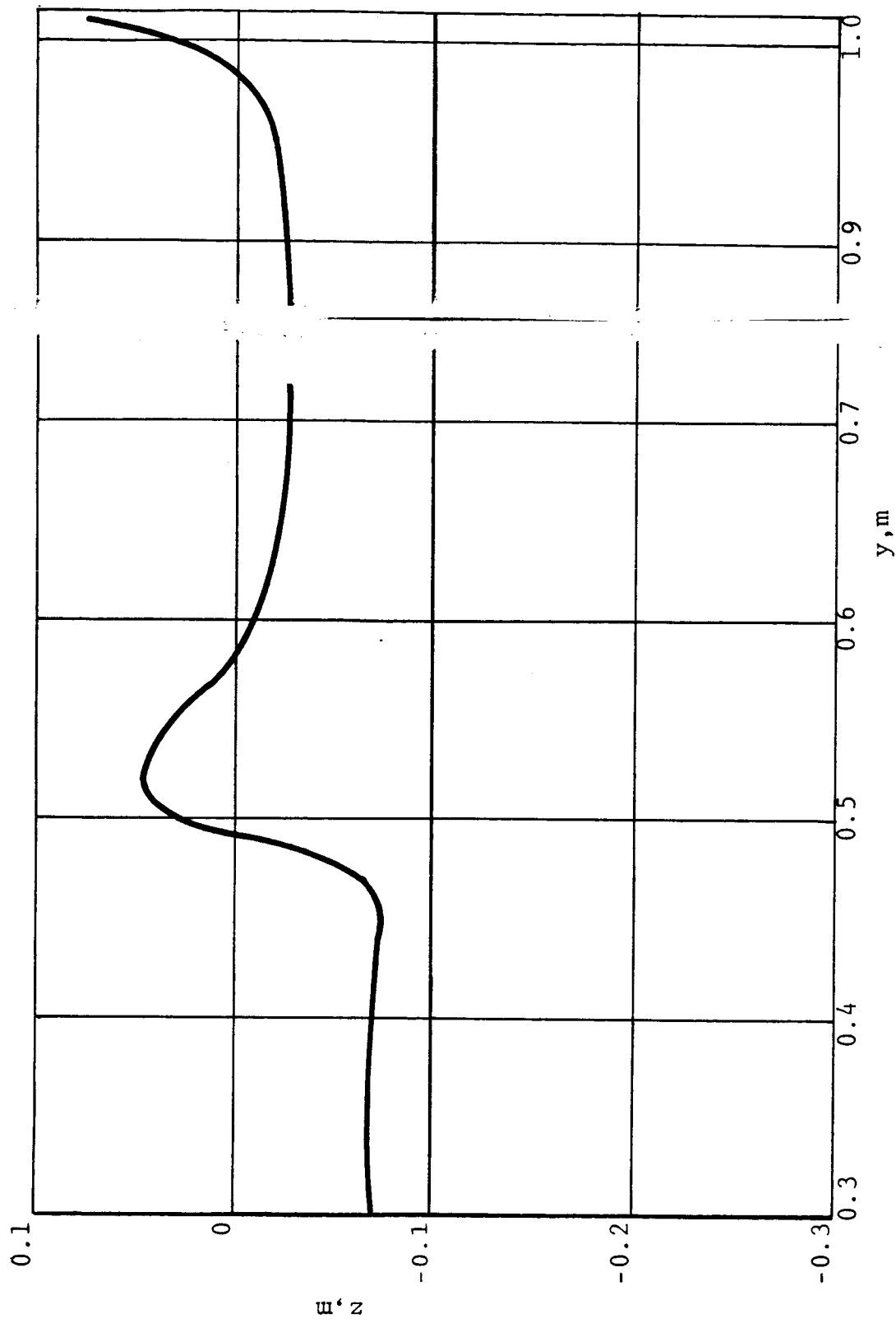Figure 24. Piecewise linear representation of typical wing with deployed flaps
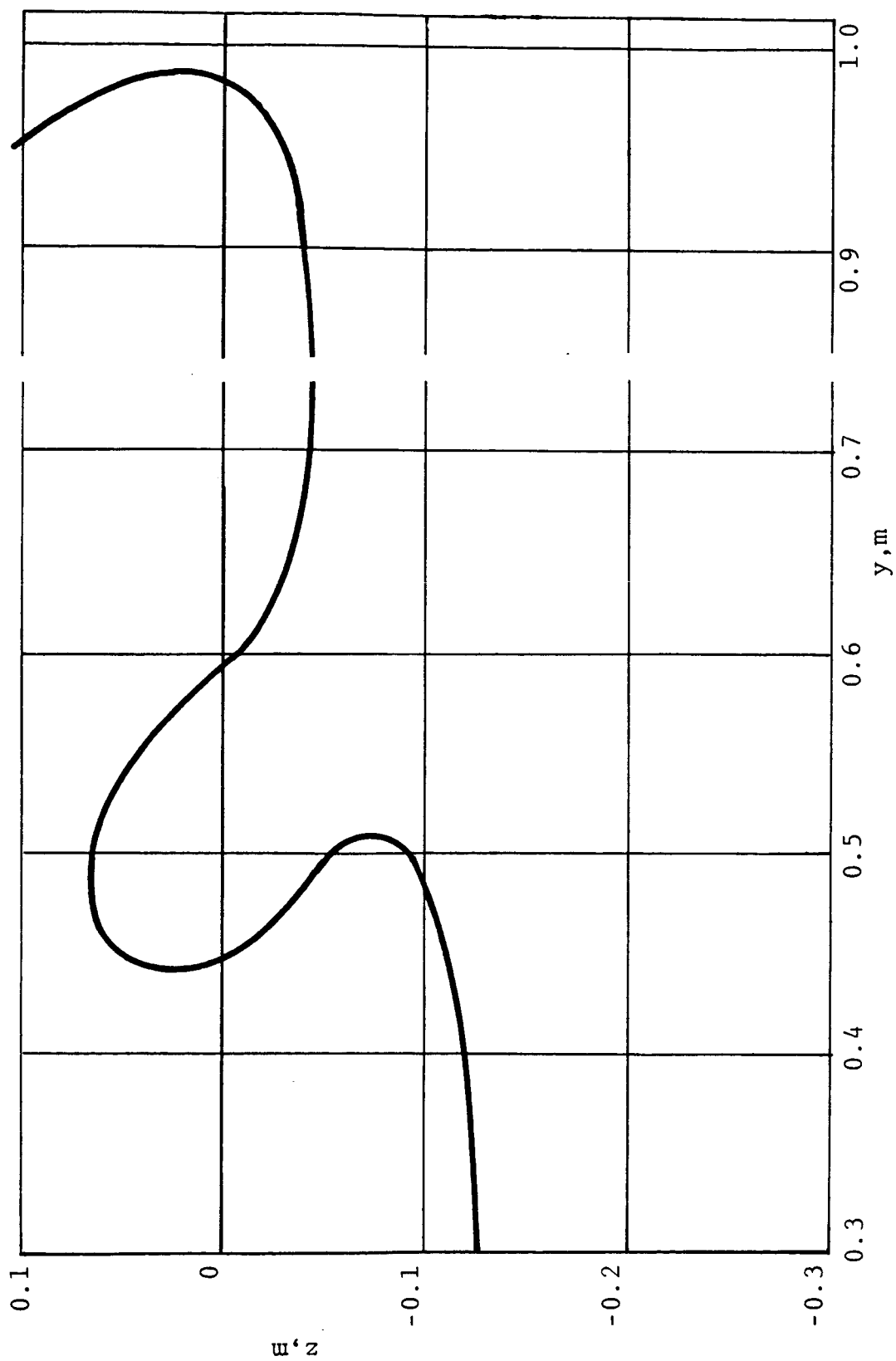
Figure 25a. Section of vortex sheet at station 0.35

Figure 25b. Section of vortex sheet at station 0.65
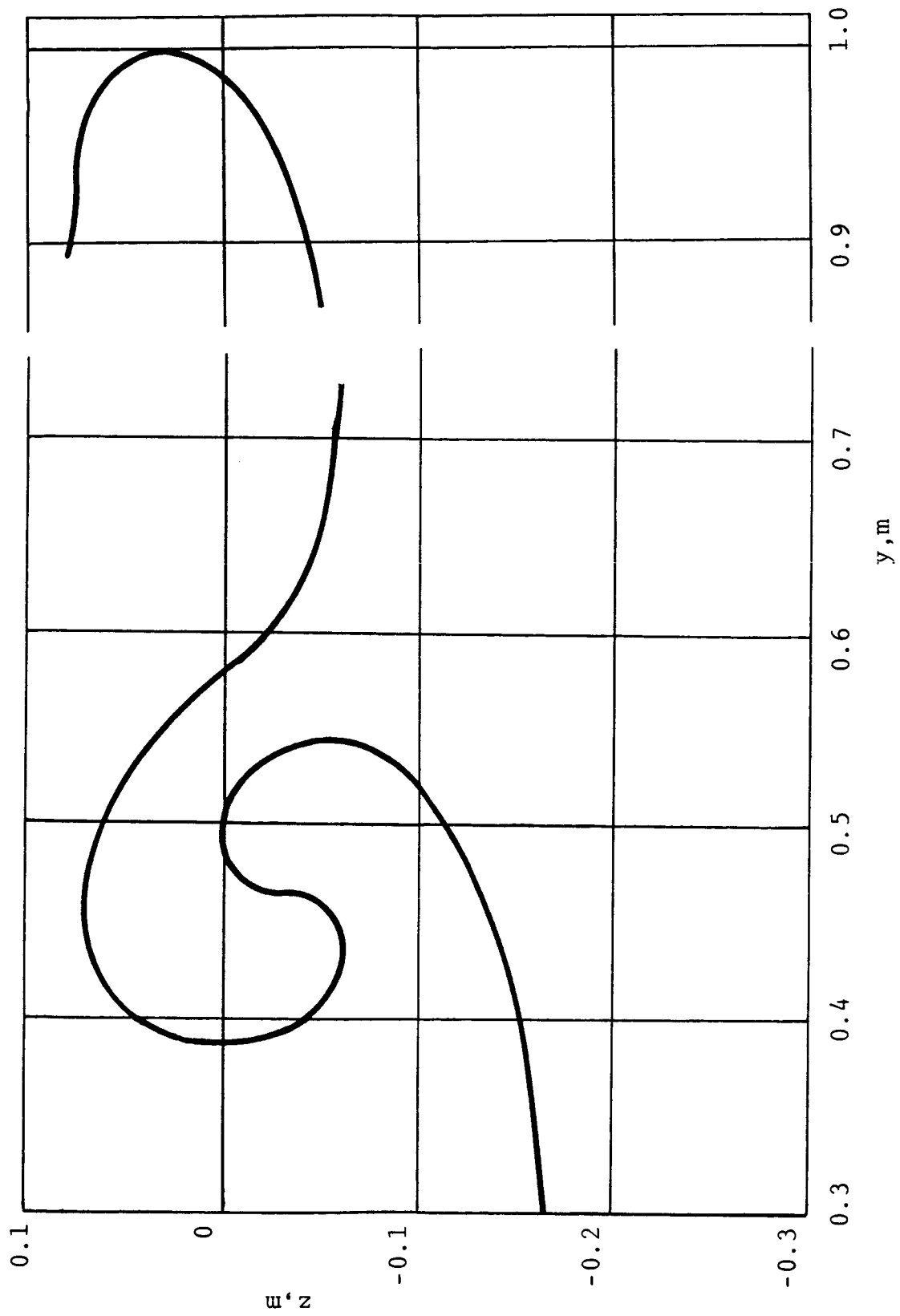
Figure 25c. Section of vortex sheet at station 0.95
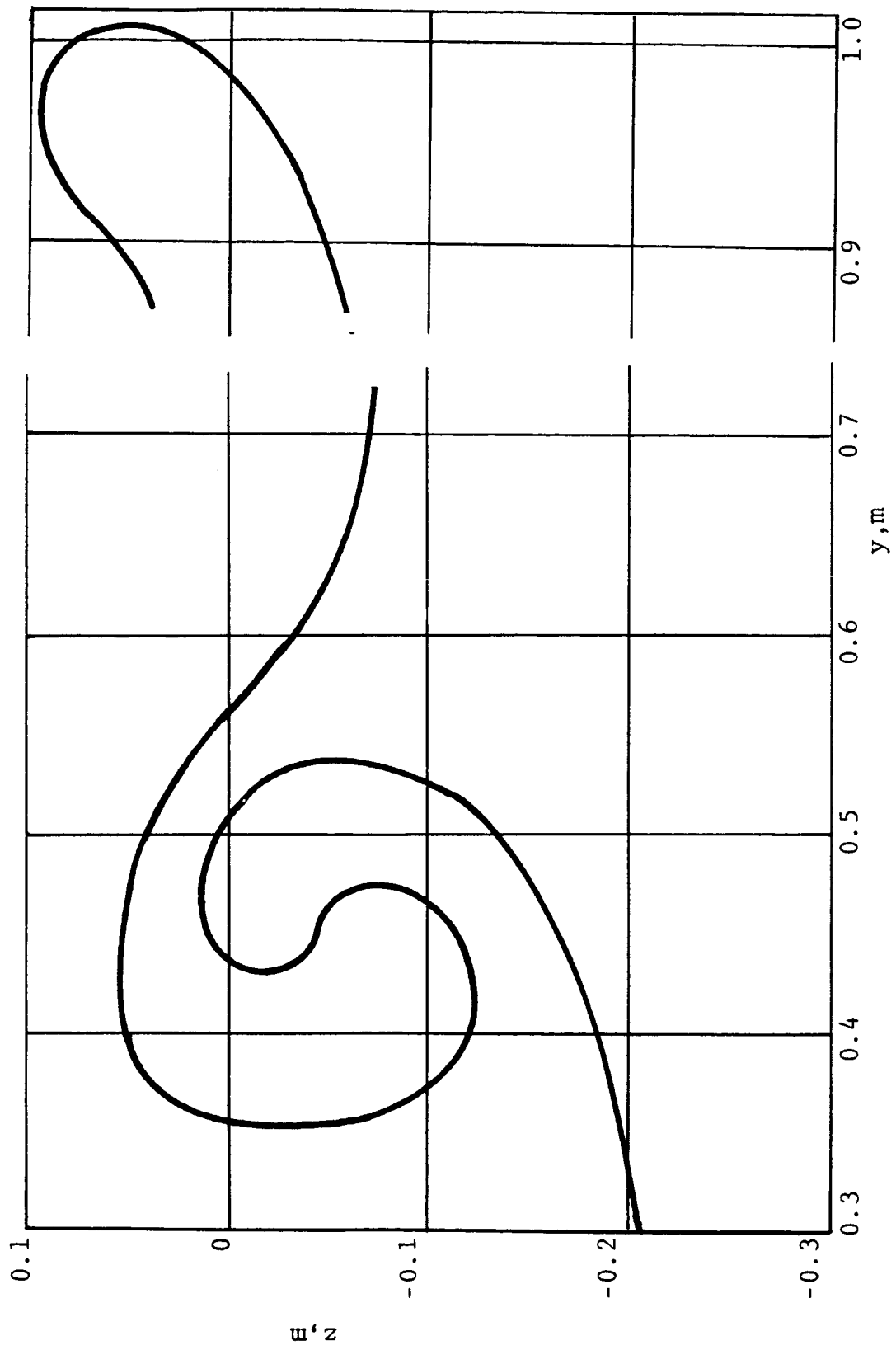
Figure 25d. Section of vortex sheet at station 1.25

Figure 25e. Section of vortex sheet at station 1.88
Solid line: as computed
Dashed line: natural shape
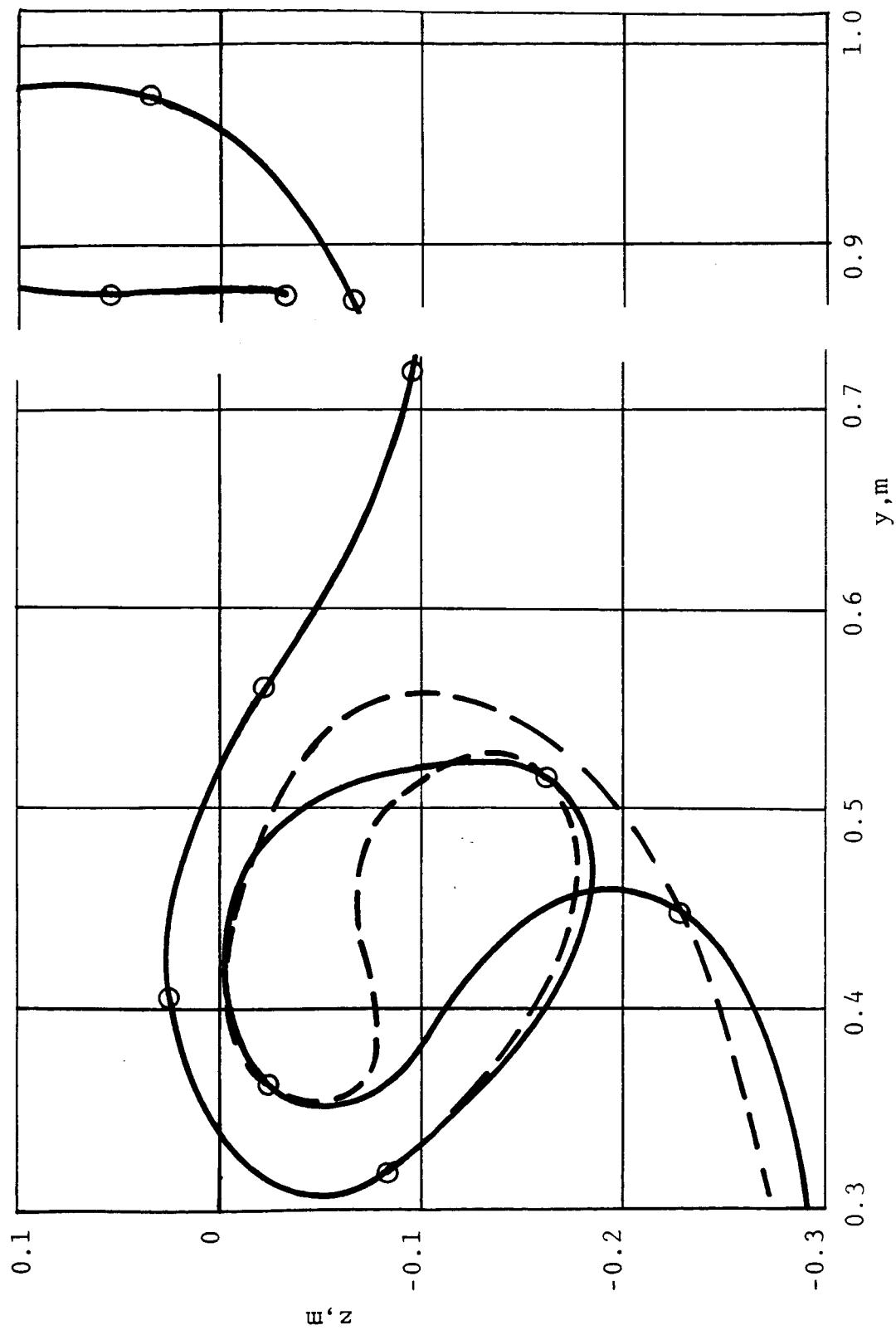
along the curve, discussed in Chapter 4 for the tip slope. If such a criterion were used at all nodes, instead of the tip only, the result may be similar to the dashed line in Figure 25e. Another way to achieve this is to increase the number of nodes to improve the fit, but at an increased computational cost.

CHAPTER VII:

CONCLUSIONS AND RECOMMENDATIONS

The objective of this study was to test the concept of using parametric bicubic patch surface definitions with bilinear vorticity or biquadratic doublet distributions, to model the vortex sheet and predict its shape numerically in the vicinity of the wing.

This choice stems from the need for continuity in these physical quantities, which is the way they occur in nature. To a full extent, this is true of the geometric representation, and to a lesser extent, it is true of the singularity distribution. For the purpose of computing induced velocities, it was shown that higher order of vorticity would not improve the truncation error. For the purpose of modeling the tip vorticity, the bilinear distribution, although satisfactory, gave rise to some difficulty. The bicubic geometric surface representation proved very suitable for curved surfaces such as the rolled-up vortex sheet, with the surface fit scheme failing only for complex wings, far downstream beyond the region of concern.

The author's opinion is that these difficulties can be surmounted by using the exact value of the velocity gradient at all the nodes of the sheet to obtain the tangent vectors in the spanwise direction. Therefore, it is suggested that

this effort be undertaken in a follow-up study. The versatility of the model may also be improved by using a more appropriate integration scheme for handling singularities. Despite these approximations, the results shown in Chapter VI amply demonstrate the quality of the approach compared to some of the schemes currently used, based on discrete, piecewise linear vortex filaments. For example, the Trefftz plane method (32) results in very tight spiral (29), and the method used by Hackett and Evans (14), which uses finite upstream filament lengths, displays excessive sensitivity to the positioning of the filaments. The present method is sensitive to node positioning only near the tip and trailng edge, and the author's opinion is that it can be alleviated by the above suggested refinements.

This method should be incorporated in a potential flow computational system for a variety of reasons.

1. It is certain to improve the *accuracy of predicting the wing loading*, following one iteration, despite the fact that tip flow is not included. In most available programs, the Kutta condition is imposed on the assumption that the streamlines at the trailing edge coincide with some arbitrary direction, for example, the bisector of the trailing edge angle. This may be acceptable as a first estimate, giving downwash angles at the trailing edge to be used for

streamline directions for the next and probably last relaxation cycle.

2. Farther from the wing, that is, near aft fuselage and empennage surfaces, the effect of rollup is necessary in many cases in attempts to *predict stability derivatives*, both longitudinal and lateral. Lateral conditions will necessitate modeling of both halves of the aircraft, which is done in potential flow solutions involving side-slip, yaw or roll rates. A *systematic, rigorous and rational evaluation* of the configuration, especially if unique and original, will be obtained, instead of attempts of intuitively adapting existing data which are not necessarily valid, potentially leading to inadequate design to be discovered only after expensive wind tunnel testing.

3. *Additional computational effort is relatively small,* except in the cases requiring re-evaluation of the entire potential flow solution, as described in 1 above. The solutions in 2 will not require reevalua-tion of the entire flow, once the wing loading has been determined, in general.

4. The usage of the parametric bicubic patch in the manner of the present study suggests it can be used to represent solid boundaries as well, for the

purpose of solving for the singularity (source) strength distributions, and hence, pressure distributions. Fewer panels will be needed than with flat panels, and the nodal spacing is not very critical due to bilinear singularities. This feature is extremely valuable for preliminary designers, and its usage is being introduced (18). The *compatibility* of such a system with the techniques of the present study is evident, and incorporation of this wake relaxation scheme can be readily implemented.

Additional experimental verification is desirable, especially for the flaps deployed case, as well as a yawed configuration. These seem to be natural extensions of the work presented here, along with the suggested refinements discussed earlier in this chapter and in Chapter VI.

BIBLIOGRAPHY

1. D. A. Anderson, J. C. Tannehill and R. H. Pletcher.
    Computational Fluid Dynamics and Heat Transfer.
    New York, N. Y.: McGraw-Hill Co., 1984.

2. H. Ashley and M. Landahl. Aerodynamics of Wings and
    Bodies. Reading, Mass.: Addison-Wesley Publishing
    Co., 1965.

3. R. E. Barnhill and R. F. Riesenfeld. Computer Aided
    Geometric Design. New York: Academic Press, 1974.

4. A. Betz. "Verhalten von Wirbelsystemen." Zeitschrift
    fur Angewandte Mathematik und Mechanik, 12, No.3
    (June 1932), 164-174 (also as NACA TM713).

5. P. Bezier. "Mathematical and Practical Possibilities of
    UNISURF." In Computer Aided Geometric Design.
    R. E. Barnhill and R. F. Riesenfeld, eds. New York:
    Academic Press, 1974.

6. D. J. Butter and G. J. Hancock. "A Numerical Method for
    Calculating the Trailing Vortex System Behind a
    Swept Wing at Low Speed." The Aeronautical Journal,
    75, No. 728 (August 1971), 564-568.

7. N. A. Chigier and V. R. Corsiglia. "Tip Vortices Velocity
    Distributions." NASA TMX-62,087, 1971.

8. C. duP. Donaldson, R. S. Snedeker and R. D. Sullivan.
    "Calculation of the Wakes of Three Transport Aircraft
    in Holding, Takeoff, and Landing Configurations and
    Comparison with Experimental Measurements." Report
    No. FAA-RD-73-42, Dept. of Transportation, March 1973.

9. Z. El-Ramly. "Aircraft Trailing Vortices-A Survey of
    the Problem". Tech. Rep. ME/A 72-1. Faculty of
    Engineering, Division of Aerothermodynamics, Carleton
    University, Ottawa, Canada, November, 1972.

10. B. M. Elson. "Pitch Control Problem Anticipated on
    Boeing 767". Aviation Week and Space Technology,
    (February 25, 1980), 25-26.

11. B. Etkin. Dynamics of Flight Stability and Control.
    New York: John Wiley and Sons, 1982.

12. I. D. Faux and M. J. Pratt. <u>Computational Geometry for Design and Manufacture</u>. New York: Ellis Horwood Ltd. Chichester, Halstead Press, Div. of John Wiley and Sons, 1979.

13. J. C. Ferguson. "Multivariable Curve Interpolation." <u>J. ACM</u>, 11, No. 2 (1964), 221-228.

14. J. E. Hackett and M. R. Evans. "Vortex Wakes Behind High Lift Wings." <u>J. Aircraft</u>, 8, No. 5 (May 1971), 334-340.

15. J. L. Hess and A. M. O. Smith. "Calculation of Non-lifting Potential Flow About Arbitrary Three-Dimensional Bodies." <u>J. of Ship Research</u>, 8, No. 2 (September 1964), 22-42.

16. J. L. Hess. "Calculation of Potential Flow about Arbitrary Three-Dimensional Lifting Bodies." McDonnell-Douglas Co. Report No. MDC J5679-01, October 1972.

17. J. L. Hess. "A Higher Order Panel Method for Three-Dimensional Potential Flow." Report No. NADC 77166-30, June 1979.

18. J. L. Hess and D. M. Friedman. "An Improved Higher Order Panel Method for Three-Dimensional Lifting Potential Flow." Report No. NADC-79277-60, December 1981.

19. J. D. Iversen, S. Park, D. R. Backhus, R. A. Brinkman and V. R. Corsiglia. "Hot-Wire, Laser Anemometer and Force Balance Measurements in Cross-Sectional Planes of Single and Interacting Trailing Vortices." <u>AIAA 11th Fluid and Plasma Dynamics Conference</u>, Seattle, Wash., AIAA paper 78-1194, July 1978.

20. F. T. Johnson and P. E. Rubbert. "Advanced Panel-Type Influence Coefficient Methods Applied to Subsonic Flows". AIAA paper 75-50, January 1975.

21. J. L. Lundry. "Development of Wake Turbulence Capability in 1975." Boeing Co. Report D6-43796TN, September 1976.

22. G. J. Peters. "Interactive Computer Graphics Application of the Parametric Bi-Cubic Surface to Engineering Design Problems." <u>Computer Aided Geometric Design</u>. R. E. Barnhill and R. F. Riesenfeld, eds. New York: Academic Press, 1974.

23. V. J. Rossow. "Survey of Computational Methods for
    Lift Generated Wakes." Conference on Aerodynamic
    Analyses Requiring Large Computers. Langley Research
    Center, Hampton, VA, March 1975. NASA SP-347.

24. V. J. Rossow. "Theoretical Study of Lift Generated
    Vortex Wakes Designed to Avoid Roll Up." AIAA J.,
    13, No. 4 (April 1975), 476-484.

25. V. J. Rossow. "Inviscid Modeling of Aircraft Trailing
    Vortices." Symposium on Wake Vortex Minimization,
    Washington, D.C., February 1976. NASA SP-409.

26. P. E. Rubbert. "Theoretical Characteristics of Arbitrary
    Wings by a Nonplanar Vortex Lattice Method." Report
    No. D6-9244, The Boeing Co., 1964.

27. P. E. Rubbert, G. R. Saaris, M. B. Scholey, N. M. Standen
    and R. E. Wallace. "A General Method for Determining
    the Aerodynamic Characteristics of Fan-in-Wing
    Configurations." Vol. 1. Theory and Application.
    Technical Report 67-61A, USAAVLABS, 1967.

28. P. E. Rubbert and G. R. Saaris. "Review and Evaluation
    of a Three-Dimensional Lifting Potential Flow Analysis
    Method for Arbitrary Configuration." AIAA paper
    72-188, January 1972.

29. D. A. Sikavi. "An Experimental and Theoretical Compara-
    tive Study of Boeing's Wake Turbulence Assessment
    System". Boeing Co. Report D6-46383TN, July 1978.

30. J. R. Spreiter and A. H. Sacks. "The Rolling Up of the
    Trailing Vortex Sheet and Its Effect on the Downwash
    Behind Wings." J. Aeronautical Sciences, 18
    (January 1951), 21-33.

31. United States Air Force. "USAF Stability and Control
    DATCOM". Flight Control Division, AFFDL, Wright-
    Patterson AFB, Ohio, 1960. (Revised 1976).

32. F. L. Westwater. "The Rolling Up of the Surface
    Discontinuity behind an Aerofoil of Finite Span."
    Reports and Memoranda 1692 - British Aeronautical
    Research Council, 1935, 116-131.

ACKNOWLEDGEMENTS

I wish to express my gratitude to the members of my committee, Professors: K. A. Heimes of Mathematics; E. S. Takle and D. N. Yarger of Earth Sciences; C. T. Hsu, J. M. Vogel, L. N. Wilson, and the Chairman, J. D. Iversen, Aerospace Engineering for the support, encouragement and knowledge they imparted in me through lectures or conferences. A great deal of appreciation is due to other Iowa State University faculty not directly involved in this dissertation, but along with committee members, contributed to my professional development and maturity.

I am also indebted to the NASA-Ames Research Center for the financial support during the Summers of 1983 and 1984.